

Application of resting-state fMRI methods to acute ischemic stroke

Dissertation

zur Erlangung des akademischen Grades

Dr. rer. med.

an der Medizinischen Fakultät

der Universität Leipzig

eingereicht von:

Master-Ingenieur Yating Lv

geboren am 07.04.1982 in Shanxi/China

angefertigt an / in:

Max-Planck-Institut für Kognitions- und Neurowissenschaften

Betreuer:

Prof. Dr. Arno Villringer

Dr. Daniel S. Margulies

Datum des Verleihungsbeschlusses der Medizinischen Fakultät: 15.10.2013

Table of Contents

Bibliographic description.....	1
List of symbols.....	3
1. General introduction.....	6
1.1. Introduction of stroke and stroke MR.....	7
1.1.1. Introduction of stroke.....	7
1.1.1.1. Stroke overlook.....	7
1.2.2.2. Stroke diagnosis.....	8
1.1.2. Stroke MRI.....	9
1.1.2.1. Diffusion-weighted imaging (DWI).....	9
1.1.2.2. Dynamic susceptibility contrast-enhanced perfusion-weighted imaging.....	11
1.1.2.3. Mismatch concept: ischemic penumbra.....	15
1.2. Introduction of resting-state functional magnetic resonance imaging and methods.....	16
1.2.1. Introduction of resting-state fMRI.....	16
1.2.2. Introduction of processing methodologies for resting-state fMRI data analysis...	18
1.2.2.1. Functional Connectivity.....	18
1.2.2.2. Independent component analysis (ICA).....	20
1.2.2.3. Clustering.....	23
1.2.2.4. Local methods.....	26
2. Study1: Tissue-Differentiation in Stroke using resting-state fMRI.....	29
2.1. Introduction.....	29
2.2. Subjects/ Materials and Methods.....	30
2.2.1. Participants.....	30
2.2.2. MR data acquisition.....	30
2.2.3. Data Analysis.....	31
2.2.3.1. Data preprocessing.....	31
2.2.3.2. Making mask.....	31
2.2.3.3. Normalization.....	33
2.2.2.4. Analysis 1 & 2: Interhemisphere comparison of power spectrum.....	33
2.2.2.5. Analysis 3: Clustering.....	33
2.3. Results.....	33
2.3.1. Results of Analysis 1 & 2: Interhemisphere comparison of power spectrum.....	33
2.3.2. Results of Analysis 3: Clustering.....	35
2.4. Discussion.....	36
3. Study 2: Identifying the perfusion deficit in acute stroke with resting-state fMRI.....	39
3.1. Introduction.....	39
3.2. Subjects/ Materials and Methods.....	40
3.2.1. Participants.....	40
3.2.2. MR data acquisition.....	40
3.2.3. Data Analysis.....	41
3.2.3.1. Data preprocessing.....	41

3.2.3.2. Time-shift analysis (TSA)	41
3.2.3.3. Clinical validation	43
3.2.3.4. Time-shift analysis (TSA) on resting-state data with reduced volumes	43
3.2.3.5. Correlateion with clinical information	43
3.3. Results	43
3.3.1. Time-shift analysis (TSA) results.....	43
3.3.2. Clinical validation results.....	50
3.3.3. Time-shift analysis (TSA) results on resting-state data with reduced volumes.....	51
3.3.4. Other results:	52
3.4. Discussion	54
4. General discussion and outlook	57
4.1. Optimization of time-shift analysis (TSA) method.....	58
4.1.1. Fast scan sequence for resting-state fMRI scanning	58
4.1.2. Other improvements for TSA optimization.....	60
4.2. Heart beat acts as bolus for measuring perfusion shifts in BOLD-fMRI	61
4.3. Other thoughts for future research	62
Summary	63
References.....	67
Acknowledgements.....	82

Bibliographic description

Lv, Yating

Application of resting-state fMRI methods to acute ischemic stroke

Universität Leipzig, Dissertation

61 pages, 127 references, 23 figures, 3 tables

Article and presentation included in this thesis:

Lv, Y., Margulies, D.S., Cameron, Craddock R., Long, X., Winter. B., Gierhake, D., Endres, M., Villringer, K., Fiebach, J., Villringer. A., 2013. Identifying the perfusion deficit in acute stroke with resting-state functional magnetic resonance imaging. *Ann Neurol* 73(1), 136-140.

Lv, Y., Margulies. D.S., Long, X., Rohr, C., Winter, B., Endres, M., Villringer, K., Fiebach, J., Villringer, A. Tissue-Differentiation in Stroke using resting-state fMRI. Poster presented at 17th Annual Meeting of the Organization for Human Brain Mapping, June 26-30, 2011, Quebec City, Canada.

Referat:

Diffusion weighted imaging (DWI) and dynamic susceptibility contrast-enhanced (DSC) perfusion-weighted imaging (PWI) are commonly employed in clinical practice and in research to give pathophysiological information for patients with acute ischemic stroke. DWI is thought to roughly reflect the severely damaged infarct core, while DSC-PWI reflects the area of hypoperfusion. The volumetric difference between DWI and DSC-PWI is termed the PWI/DWI-mismatch, and has been

suggested as an MRI surrogate of the ischemic penumbra. However, due to the application of a contrast agent, which has potentially severe side-effects (e.g., nephrogenic systemic fibrosis), the DSC-PWI precludes repetitive examinations for monitoring purposes. New approaches are being sought to overcome this shortcoming.

BOLD (blood oxygen-level dependent) signal can reflect the metabolism of blood oxygen in the brain and hemodynamics can be assessed with resting-state fMRI. The aim of this thesis was to use resting-state fMRI as a new approach to give similar information as DSC-PWI. This thesis comprises two studies:

In the first study (see Chapter 2), two resting-state fMRI methods, local methods which compare low frequency amplitudes between two hemispheres and a k-means clustering approach, were applied to investigate the functional damage of patients with acute ischemic stroke both in the time domain and frequency domain. We found that the lesion areas had lower amplitudes than contralateral homotopic healthy tissues. We also differentiated the lesion areas from healthy tissues using a k-means clustering approach.

In the second study (see Chapter 3), time-shift analysis (TSA), which assesses time delays of the spontaneous low frequency fluctuations of the resting-state BOLD signal, was applied to give similar pathophysiological information as DSC-PWI in the acute phase of stroke. We found that areas which showed a pronounced time delay to the respective mean time course were very similar to the hypoperfusion area.

In summary, we suggest that the resting-state fMRI methods, especially the time-shift analysis (TSA), may provide comparable information to DSC-PWI and thus serve as a useful diagnostic tool for stroke MRI without the need for the application of a contrast agent.

List of Symbols

ACI	Internal carotid artery
AD	Alzheimer disease
ADC	Apparent diffusion coefficient
ADHD	Attention deficit hyperactivity disorder
AFNI	Analysis of Functional NeuroImaging
ALFF	Amplitude of low frequency fluctuations
ASL	Arterial spin labeling
BOLD	Blood oxygen-level dependent
CBF	Cerebral blood flow
CBV	Cerebral blood volume
CC	Correlation coefficient
CEN	Central-executive network
CSF	Cerebrospinal fluid
CCT	Cranial computed tomography
DC	Dice coefficient
DMN	Default mode network
DSC –PWI	Dynamic susceptibility contrast-enhanced perfusion-weighted imaging
DWI	Diffusion weighted imaging
ECG	Electrocardiogram
EPI	Echo planar imaging
FA	Flip angle
fALFF	Fractional amplitude of low frequency fluctuations

FLAIR	Fluid attenuated inversion recovery
FSL	FMRIB Software Library
FWHM	Full width at half maximal
ICA	Independent component analysis
ICs	Independent components
IPC	Inferior parietal cortex
LFF	Low-frequency fluctuations
LFO	Low frequency oscillations
LFPs	Local field potentials
MB	Multibanded Radio frequency pulses
MCA	Middle cerebral artery
MCI	Mild cognitive impairment
MNI	Montreal Neurological Institute
MPC	Maximal peak concentration
MPFC	Medial prefrontal cortex
MRI	Magnetic resonance imaging
MTT	Mean transit time
NIHSS	National Institutes of Health Stroke Scale
NIRS	Near-infrared spectroscopy
PCA	Posterior cerebral artery
PCC	Posterior cingulate cortex
PET	Positron emission tomography
ReHo	Regional homogeneity
ROI	Region-of-interest

rsfMRI	Resting-state functional magnetic resonance imaging
rtPA	Recombinant tissue Plasminogen Activator
sICA	Spatially independent component analysis
SIR	Simultaneous echo refocused
SNR	Signal-to-noise ratio
SPECT	Single-photon emission computed tomography
SPM	Statistical parametric mapping
TE	Echo time
TIA	Transient ischemic attack
TR	Repetition time
TSA	Time-shift analysis
TTP	Time to peak
WHO	World Health Organization

1. General Introduction

As the second leading cause of death and major cause of disability in the world (Donnan et al., 2008; Mathers et al., 2009), stroke is the rapid loss of brain function due to disturbance in the blood supply to the brain. Stroke can cause permanent neurological damage, complications, and death. Acute ischemic stroke is caused by the blockage of blood vessel in the brain. Therapeutic decisions must be made quickly after stroke onset, where minutes can make the difference between benefit and harm to the patient. The rapid diagnosis is crucial for patient outcome after stroke onset. Diffusion weighted imaging (DWI) and dynamic susceptibility contrast-enhanced (DSC) perfusion-weighted imaging (PWI) are commonly employed in clinical practice and in research to give pathophysiological information for patients with acute ischemic stroke (Sorensen et al., 1996; Wardlaw, 2010; Merino and Warach, 2010; Dani et al., 2011). DWI is thought to roughly reflect the severely damaged infarct core due to cytotoxic edema which is caused by the breakdown of sodium-potassium pumps, while DSC-PWI reflects the area of hypoperfusion due to hemodynamic compromise in the brain. The volumetric difference between DWI and DSC-PWI is termed the PWI/DWI-mismatch, and has been suggested as an MRI surrogate of the ischemic penumbra (Karonen et al., 1999; Schlaug et al., 1999) (Fig 1.1). The cerebral blood flow (CBF) damage in the mismatch area is potentially reversible. If normal CBF is restored in time, the ischemic damage in the penumbra can be minimized, otherwise long-term hypoperfusion in penumbra will eventually lead to infarction. Therefore the ischemic penumbra is regarded as the prime target for any treatment approach after acute ischemic stroke onset.

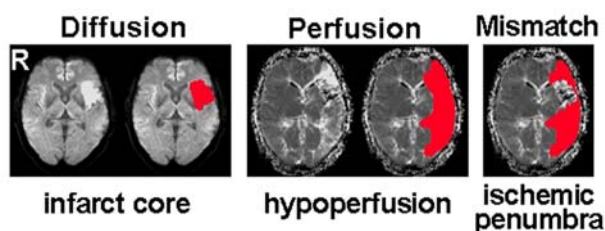


Figure 1.1: An example of DWI, DSC-PWI and PWI/DWI-mismatch area.

However, the mismatch concept for identifying the penumbra has been challenged as being frequently inaccurate due to the lack of good quantification of perfusion at low

perfusion levels and its susceptibility to alterations of the arterial input. Due to the application of a contrast agent, which, though effective to induce a transient change in MRI signal due to magnetic susceptibility effects (Villringer et al., 1988), has potentially severe side-effects (e.g., nephrogenic systemic fibrosis), the DSC-PWI precludes repetitive examinations for monitoring purposes. New approaches are being sought to overcome this shortcoming.

Resting-state functional magnetic resonance imaging (rsfMRI) is a noninvasive imaging technique which does not require contrast agent application and is of relatively low cost, while still maintaining high temporal resolution. Therefore, the resting-state fMRI is increasingly applied to research questions regarding brain disorders (Li et al., 2002; Greicius et al., 2004). BOLD (blood oxygen-level dependent) signal can reflect the metabolism of blood oxygen in the brain and hemodynamics can be assessed with resting-state fMRI (Tong et al., 2010).

The aim of this thesis is try to use resting-state fMRI as a new approach to give similar information as DSC-PWI. Specifically, we aim to apply the resting-state fMRI approach to differentiate the lesion area from healthy tissues in patients with acute ischemic stroke.

1.1. Introduction of stroke and stroke MRI

1.1.1. Introduction of stroke

1.1.1.1. Stroke overlook

The definition of stroke from the World Health Organization (WHO) is: a clinical syndrome characterized by rapidly developing clinical symptoms and / or signs of focal, and at times global (applied to patients in deep coma and those with subarachnoid hemorrhage), loss of cerebral function, with symptoms lasting more than 24 hours or leading to death, with no apparent cause other than that of vascular origin. Simply, a stroke is the rapid loss of brain function due to disturbance in the blood supply to the brain.

Stroke can cause permanent neurological damage, complications, and death. Stroke prevention is a primary goal of community and personal health programs. Stroke has become the second leading cause of death and major cause of disability in the world (Donnan et al., 2008; Mathers et al., 2009). Identification of stroke risk factors and implementation of activities to eliminate or diminish their impact are essential to the reduction of stroke morbidity and mortality (WHO Task Force, 1989). In the report of the WHO Task Force on stroke and other Cerebrovascular Disorders, it is pointed out that stroke risk factors include arterial hypertension, diabetes mellitus, heart disease, transient ischemic attack (TIA) and completed stroke, obesity, platelet hyperaggregability, alcoholism, smoking, elevated blood lipid levels, hyperuricemia, infections, as well as genetic and familial factors. It also reported that risk factor reduction is an important step in preventing stroke and becomes an imperative for clinicians and public health officers to address (WHO Task Force, 1989).

Strokes can be classified into two major categories: ischemic stroke and hemorrhagic stroke. An ischemic stroke is caused by temporary or permanent occlusion or stenosis of a feeding artery, extracranially or intracranially, or (more rarely) of a vein or dural sinus, while a hemorrhagic stroke is the result of the rupture of an artery (e.g., due to an aneurysm or an arteriovenous malformation) or arteriole in the brain parenchyma. It is difficult to distinguish clinically between ischemic and hemorrhagic stroke, and their relative occurrence varies from country to country (WHO Task Force, 1989; Donnan et al., 2008).

1.1.1.2. Stroke diagnosis

Therapeutic decisions must be made quickly after stroke onset, minutes can make the difference between benefit and harm to the stroke patient. Immediate stroke diagnosis is extremely important after stroke onset and is typically achieved by a combination of neurological examination and neuroimaging.

The most widely used stroke scale for neurological examination is the National Institutes of Health Stroke Scale (NIHSS). The NIHSS measures stroke severity by assessment of several aspects including level of consciousness, paresis, aphasia, sensory symptoms, facial palsy, limb movement ability, dysarthria and so on. The NIHSS scores range from 0 (no symptoms) to 42 (maximum points in all categories). If the NIHSS score is larger than 25 the stroke patient is in a serious medical

condition.

Neuroimaging is used to determine subtypes and causes of stroke. The most commonly used imaging techniques for acute ischemic stroke diagnosis in the clinic are cranial computed tomography (CCT) and magnetic resonance imaging (MRI). While in most hospitals CCT is performed due to its widespread availability and ease of use, MRI provides more detailed pathophysiological information and is becoming more and more important. In the following I will introduce stroke MRI techniques which are of interest to our study.

1.1.2. Stroke MRI

For diagnosing acute ischemic stroke, stroke MRI which includes fluid attenuated inversion recovery (FLAIR), T2*-weighted imaging, diffusion weighted imaging (DWI), and dynamic susceptibility contrast-enhanced (DSC) perfusion-weighted imaging (PWI) is commonly employed to provide detailed pathophysiological information of the affected brain areas.

1.1.2.1. Diffusion-weighted imaging (DWI)

Molecular diffusion refers to the random translational motion of molecules, also called Brownian motion, that result from the thermal energy carried by these molecules (Le Bihan et al., 2001). In the human brain, water molecules are constantly in random motion in gray matter or cerebrospinal fluid (CSF) which means the diffusion is the same in all direction. In white matter, however, there are barriers to water molecules diffusion, such as membranes, which the molecules cannot readily penetrate. This causes diffusion to be anisotropic, i.e., diffusion is faster in some directions than others. The diffusion path of water molecules therefore reflects the structure of human brain (gray matter, white matter and CSF) due to the different diffusion property in these tissues.

Diffusion-weighted imaging (DWI) can measure the Brownian motion of water molecules. The sequence was first described by Stejskal and Tanner (Stejskal and Tanner, 1965). They applied a spin echo sequence coupled with a symmetric gradient

pulse, which could measure the displacement of water molecules in a direction of a period of time. The acquisition time of this sequence was 6–8 minutes and could only measure the diffusion in one direction (Stejskal and Tanner, 1965). After the introduction of ultrafast echo planar imaging (EPI) by Mansfield (Mansfield, 1977; Mansfield, 1984), the measurement of water diffusion with imaging methods became possible. EPI is the fastest scanning techniques in clinical applications. It shortens considerably the time required to form an image: within 30ms it can acquire a single image and within tens of seconds it can collect the native spatial data, which is required for image reconstruction. The benefits of rapid data collection using EPI are indispensable in collecting water diffusion image despite the lower signal-to-noise ratio (SNR). The first whole-body diffusion images were acquired by Le Bihan and colleagues (Le Bihan, et al., 1986; Le Bihan, et al., 1988). Moseley and colleagues were the first to demonstrate the clinical importance of diffusion imaging by detecting ischemic tissue within minutes after onset of a stroke in an experimental animal model (Moseley et al., 1990). Warach and colleagues were first to detect human ischemia by using diffusion imaging (Warach et al., 1992).

In the presence of a magnetic field gradient, the transverse magnetization of protons who experience different magnetic field strengths get “out of phase” resulting in an attenuation of the MR signal. This attenuation depends on the diffusion coefficient and the strength of the magnetic field gradient. The signal loss (S/S_0) is mathematically described as follows:

$$\frac{S}{S_0} = e^{-b \cdot ADC} \quad (1)$$

Where S_0 represents signal intensity when $b = 0$; b is a diffusion-sensitive factor, also called b-value, which is calculated as: $b = \Gamma^2 G^2 \delta^2 (\Delta - \delta / 3)$. The b-value is a sequence-specific variable and depends on the gyromagnetic ratio (Γ), the strength of the diffusion gradient (G), the duration of the gradient pulse (δ) and the time interval between both gradient pulses (Δ). The apparent diffusion coefficient (ADC) is a tissue-specific variable which can reflect the structure characteristics of the tissue. The ADC represents the water molecular movement along the direction of the diffusion gradient. When the ADC value is increased, representing an increase of water diffusion, the DWI signal is lower, and vice versa.

Due to the alteration of water diffusion in the ischemic infarct area, DWI is now

commonly applied in the clinic to detect the ischemia. Indeed, DWI is very sensitive to detect signs of acute cerebral ischemia. In acute stroke, due to cytotoxic edema, which is caused by the breakdown of sodium-potassium pumps, DWI can detect signs of brain damage earlier than T2 weighted imaging. The presence of cytotoxic edema indicates that the sodium - potassium pumps have lost normal function, extracellular water has entered the cell, and intracellular water is increased. Since diffusion of intracellular water is more restricted than that of extracellular water due to diffusion-limiting structures such as cell membranes and microparticles, this leads to an overall decline of the diffusion coefficient and hence an increased signal on DWI in ischemic area. Figure 1.2 gives an example of DWI in a patient with acute ischemic stroke. The area with higher intensity in DWI reflects the infarct core (Fig 1.2).

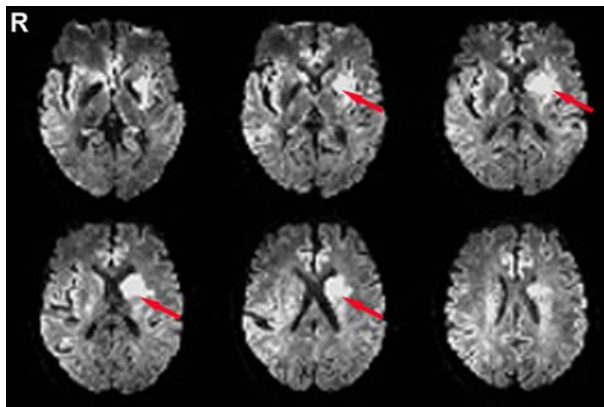


Figure 1.2 DWI in acute ischemic stroke: the area with higher signal intensity (red arrow) indicates the infarct core.

1.1.2.2. Dynamic susceptibility contrast-enhanced perfusion-weighted imaging (DSC-PWI)

The term perfusion refers to blood passing through the capillary network where exchange of oxygen and nutrients to the tissue cells occurs. Perfusion imaging is an imaging technique which is built on the basis of this flow effect. Perfusion imaging techniques have become important in diagnosis and treatment in clinical practice of several clinical entities.

In magnetic resonance imaging, there are two common methods for perfusion imaging: One method uses MR pulse sequences which are sensitive to the movement of water molecules. The basic idea is to use water protons as an endogenous tracer. This

method is known as arterial spin labeling (ASL). Another method is based on the use of an injected contrast agent that changes the magnetic susceptibility of blood and thereby the MR signal which is repeatedly measured during the first-pass of the contrast agent bolus. This method is known as dynamic susceptibility contrast-enhanced perfusion-weighted imaging (DSC-PWI).

ASL uses water molecules in blood as intrinsic diffusion marker, the proton spins of the arterial water are labeled by changing the magnetic state prior to reaching the imaged volume. When the labeled spins enter the imaged region after a time delay, the labeled blood spins exchange with unlabelled spins in the tissue and a “labeled” image is acquired (Alsop and Detre, 1996). The signal from a given voxel in the labeled image represents a sum over both blood and tissue spins. The exchanging process leads to decreased signal in the tissue. In addition to the “labeled” image, a “control” image is acquired without labeling the arterial water spins. The local blood flow perfusion can be quantitatively determined by comparing between the “labeled” image and the “control” image (Borogovac and Asllani, 2012). ASL does not require injection of a contrast agent, and the values of blood flow can be obtained quantitatively. However, if the time delay until the labeled spins reach the imaged volume is long (as it is the case in stroke), the signal decays dramatically resulting in poor signal-to-noise ratio. Therefore, particularly in the situation of an acute ischemic stroke which is characterized by delayed blood perfusion, ASL has a poor signal-to-noise ratio and relatively low spatial resolution.

Dynamic susceptibility contrast-enhanced perfusion-weighted imaging (DSC-PWI) technique can track the signal change in the area of interest by injecting a paramagnetic contrast agent as an intravenous bolus (Villringer et al., 1988; Rosen et al., 1990). When the contrast agent passes through the vascular system of the brain, the difference in magnetic susceptibility between the spaces within and outside the capillaries will establish local magnetic field gradients. This local magnetic field heterogeneity leads to the above mentioned dephasing of protons and a pronounced signal drop in T2- and T2*-weighted MR pulse sequences. i.e. the so-called "negative enhancement". The development of fast echo planar imaging (EPI) has made it possible to image the entire brain and allow to observe the transit of the contrast agent bolus through the brain at a temporal resolution of about one second. DSC-PWI is characterized by good signal-to-noise ratio and reflects microvascular perfusion of the

brain tissue.

The signal decrease in brain tissue after contrast agent injection is a function of the local cerebral blood volume (CBV). The signal-time curve is used to determine the contrast agent concentration-time curve which is given in Figure 1.3 (Wardlaw, 2010). The concentration of the contrast agent is calculated as follows:

$$C(t) \propto \ln \frac{S(t)}{S_0} \quad (2)$$

where $C(t)$ is the contrast agent concentration in the tissue, $S(t)$ is the signal intensity and S_0 is the signal intensity before arrival of the bolus (Rosen et al., 1990).

The blood supply and hemodynamic changes of the brain tissue can be extracted from the perfusion concentration-time curve, and thus information on regional cerebral hemodynamics can be obtained. Some important physiological and pathophysiological parameters can be calculated: relative regional cerebral blood volume (CBV) can be simply calculated as proportional to the area under the contrast agent concentration-time curve; mean transit time (MTT) is calculated as $\int_0^{\infty} tC(t)dt / \int_0^{\infty} C(t)dt$, the normalized first moment of the concentration-time curve; the relative regional cerebral blood flow (CBF) is CBV/MTT . These three parameters are linked by the equation $CBV = CBF \times MTT$ as illustrated in Figure 1.3. In addition, other parameters have been derived which also describe the hemodynamic status of the brain tissue, such as the time from bolus arrival to maximal peak concentration (MPC), i.e., time to peak (TTP) and the full width at half maximal (FWHM) of the concentration-time curve (Fig 1.3).

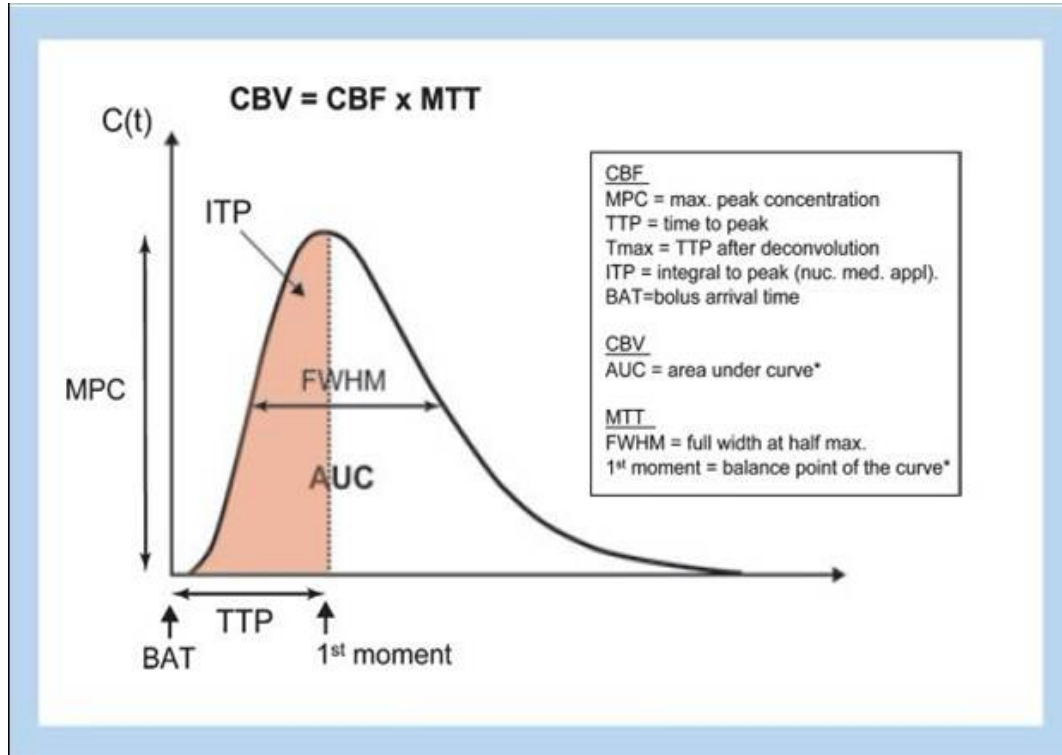


Figure 1.3 Concentration-time curve obtained during the first pass of a contrast agent bolus through the brain in DSC-PWI (Wardlaw, 2010).

For the evaluation of acute ischemic stroke, usually, the most frequently used parameters are MTT, CBF, and CBV. Especially MTT is very sensitive to brain ischemic lesions. Due to the blockage of arterial inflow into the ischemic area, the passage of blood through the brain is prolonged and therefore, MTT in the ischemic lesion area is longer than the contralateral values in normal tissues (Latchaw et al., 2009). Figure 1.4 gives MTT maps of a patient with acute ischemic stroke: the area with higher intensity is the hypoperfused area (Fig 1.4).

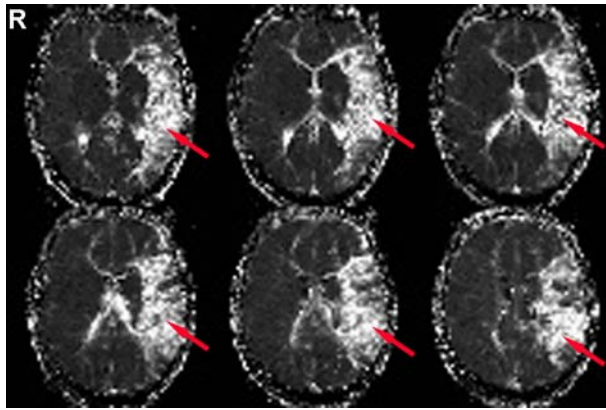


Figure 1.4 A MTT map from DSC-PWI: the area with higher intensity (red arrow) indicates the area of hypoperfusion.

The major drawback of DSC-PWI is that it requires the application of a susceptibility contrast agent which comes with potentially severe side-effects (nephrogenic systemic fibrosis) and precludes repetitive examinations for monitoring purposes.

1.1.2.3. Mismatch concept: ischemic penumbra

The occlusion of an arterial vessel will lead to a decrease in cerebral blood flow in the affected brain regions. All these areas will be identified by perfusion weighted imaging. In those areas which are most heavily affected, cytotoxic edema will occur which is identified by diffusion weighted imaging. The difference between those two is termed “mismatch” or “tissue at risk”. It is a MR surrogate parameter of the ischemic penumbra (Schellinger et al., 2001). If reperfusion occurs in time, this area may be saved or damage is minimized, if no reperfusion occurs, this area may undergo permanent damage, i.e. infarction. Reperfusion can either occur spontaneously or it may be induced by thrombolysis with recombinant tissue Plasminogen Activator (rtPA). The relationship between tissue and risk, reperfusion and damage is illustrated in Figure 1.5.

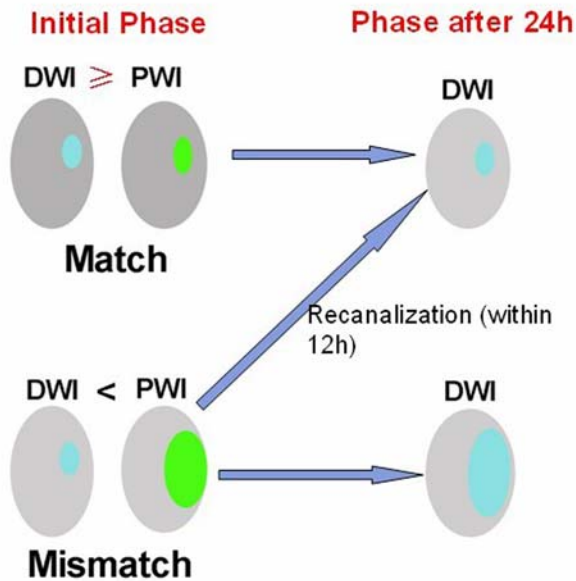


Figure 1.5 Illustration of mismatch concept after acute ischemic stroke onset.

1.2. Introduction of resting-state functional magnetic resonance imaging and methods

1.2.1. Introduction of resting-state fMRI

Since the advent of BOLD (blood oxygenation-level dependent) functional magnetic resonance imaging (fMRI) (Ogawa et al., 1990; Kwong et al., 1992), research efforts concentrated mostly on identifying regions activated by performance of a cognitive task or by administration of a stimulus. Such a stimulus-response pattern is central to cognitive neuroscience research. Through such studies we can understand localized brain involvement in a cognitive function as well as the pathological functions associated with brain disorders. In this task-based model of fMRI, the resting-state was used as baseline control state.

Resting-state is a condition in which the participant does not perform any active task and is instructed to remain still and not think of question systematically or try not to think of any questions, with eyes closed or open while fixating a cross. Although there

is still some controversy about the “functional meaning” of the resting-state, a large number of studies have shown that the BOLD signal which is measured by resting-state fMRI (rsfMRI) is of physiological and pathological importance.

Biswal and colleagues found that the presence of synchronized low-frequency fluctuations (LFF) (0.01-0.08 Hz) could be used to assess functional connectivity between left and right primary motor areas in baseline resting-state (Biswal et al., 1995). The functional connectivity patterns were very similar to activation maps during bilateral hand movement. It was concluded that the low-frequency fluctuation of BOLD signal in resting-state was neurophysiologically significant (Biswal et al., 1995). Similar functional connectivity between bilateral symmetrical regions in the brain is also present in bilateral auditory cortex (Cordes et al., 2001), bilateral visual cortex (Lowe et al., 1998; Kiviniemi et al., 2000; Kiviniemi et al., 2004; Cordes et al., 2000), bilateral amygdala (Lowe et al., 1998), bilateral thalamus (Stein et al., 2000), bilateral hippocampus (Stein et al., 2000), as well as the language network, including Broca’s and Wernicke’s areas (Hampson et al., 2002). In several studies a decreased functional connectivity of low-frequency fluctuations in resting-state was reported. For example, Li and colleagues found that the synchronization of the low-frequency fluctuations within the hippocampus decreased in Alzheimer disease (AD) (Li et al., 2002). Greicius and colleagues (Greicius et al., 2004) found the functional connectivity of rsfMRI data between motor task blocks decreased in mild cognitive impairment (MCI) among default mode network (DMN), which included the following brain areas: posterior cingulate cortex (PCC), medial prefrontal cortex (MPFC) and hippocampus etc. For both neurologists and patients, resting-state fMRI was easy to operate and compare among different studies when compared to task fMRI. Unlike positron emission tomography (PET) or single-photon emission computed tomography (SPECT) which requires injection of radionuclide into the patient’s body, resting-state fMRI does not require radionuclides and is of relatively low cost, while still maintaining high temporal resolution. Therefore, resting-state fMRI was increasingly applied to research questions regarding brain disorders.

The neural processes which are reflected in low-frequency oscillations in resting-state fMRI are still not fully understood. In addition to lots of indirect evidences about the relationship between low-frequency fluctuations (LFF) of BOLD signal in resting-state fMRI and spontaneous neural activity (Biswal et al., 1997a; McCormick,

1999; Li et al., 2002; Leopold et al., 2003), some studies have provided more direct evidences. Logothetis and colleagues (Logothetis et al., 2001) simultaneously recorded local field potentials (LFPs) of neural activity, the single- and multi-unit spiking activity, as well as fMRI BOLD signal from the visual cortex of monkeys. They found that LFPs yield a better estimate of BOLD responses than the multi-unit responses. The results suggested that BOLD signal reflects the energetically expensive synaptic activity such as that related to the LFP signals. Another study which recorded spontaneous BOLD signal in different visual cortical layers of rats found highest BOLD signal in the deeper layers during resting-state, particularly layer 4 which has higher spontaneous neuronal activity and lower synaptic density (Pelled and Goelman, 2004).

1.2.2. Introduction of processing methodologies for resting-state fMRI data analysis

As mentioned above, the low frequency fluctuations (LFF) of BOLD signal in resting-state fMRI directly reflect spontaneous neuronal activity. In the past decades, with the increasing application of resting-state fMRI in research, the analytic methodologies for resting-state fMRI data, which describe and summarize the functional organization of the brain, have increased dramatically.

1.2.2.1. Functional Connectivity

Functional connectivity is a widely used approach in resting-state fMRI data analysis. Seed-based functional connectivity analysis is the most commonly used method, which calculates the correlation between the average time course of an a priori region-of-interest (ROI), or “seed region”, and the time course of all other voxels in the brain.

The seed-based functional connectivity analysis was first applied to resting-state fMRI data by Biswal and colleagues (Biswal et al., 1995). They used a seed region in the motor cortex to perform seed-based functional connectivity analysis and found that resting-state functional connectivity map showed similar patterns to activation maps obtained with bilateral hand movement. Early studies of resting-state functional connectivity analysis focused on describing neural systems including: the motor

network (Lowe et al., 1998; Xiong et al., 1999), the visual cortical network (Cordes et al., 2000; Lowe et al., 2000; Hampson et al., 2004), the language network (Hampson et al., 2002). Greicius and colleagues (Greicius et al., 2003) were the first to use seed-based functional connectivity analysis by seeding a region in the posterior cingulate cortex (PCC) and found that PCC showed significant resting-state connectivity with medial prefrontal cortex (MPFC) and bilateral inferior parietal cortex (IPC). These regions comprise the default mode network (DMN) which had been proposed by Raichle and colleagues (Raichle et al., 2001) based on PET studies. Raichle and colleagues found that the regions in DMN exhibit higher metabolic activity or are more active than other brain regions in resting-state brain (Raichle et al., 2001).

While these initial studies were focused on studying functional connectivity of established brain network system in the absence of any cognitive task, more recent research into resting-state functional connectivity has taken advantage of its strengths in order to address topics that are beyond the practical scope of task-based fMRI (Margulies et al., 2010). For example, Margulies and colleagues (Margulies et al., 2009) used functional connectivity analysis to detect the functional subdivisions within the precuneus in both humans and monkeys. They found three distinct patterns of functional connectivity within the precuneus of both species, with each subdivision suggesting a discrete functional role. Their finding provided support that resting-state functional connectivity may reflect underlying anatomy (Margulies et al., 2009). Similar analysis has been performed with placement of seed regions throughout particular brain regions to detect subdivisions including: subdivisions detection in anterior cingulate cortex (Margulies et al., 2007), striatum (Di Martino et al., 2008), amygdala (Roy et al., 2009), medial temporal lobe (Kahn et al., 2008), and cerebellum (Krienen and Buckner, 2009). All these studies suggest that functional connectivity analysis of resting-state data is an effective method to study functional neuroanatomy.

Another commonly used approach is to correlate the average time course of several pre-selected ROIs distributed in different brain areas. Calculating the correlation matrix between a set of ROIs from resting-state data is the foundation of more advanced graph theory-based techniques. Graph theory is a well-developed mathematical tool whose aim is to characterize various aspects of a network structure

and provide tools to describe aspects of the network configuration itself (Diestel, 2005; Achard et al., 2006)

Another method named effective connectivity, as opposed to functional connectivity, which addresses causal interactions between different brain regions using fMRI data. Sridharan and colleagues (Sridharan et al., 2008) applied Granger causality analysis in fMRI data, which could elucidate the dynamic interactions between selected regions based on temporal precedence of time courses, and found that right fronto-insular cortex is likely to play a critical and causal role in switching between the central-executive network (CEN) and the default mode network (DMN) in three task states. Granger causality analysis was also used on resting-state fMRI data to address interaction of the default-mode network (Uddin et al., 2009). However, Smith and colleagues pointed that the lag-based fMRI causality analysis may be biased by hemodynamic variability and the lack of this variability confound for the studied brain regions should be demonstrated when interpreting the lag-based causality results (Smith et al., 2012a).

In summary, functional connectivity analysis is one of the primary analytic strategies for resting-state data. The straightforward statistics and comprehensible results have made it a widely applied technique. However, its primary drawback is high dependence upon selecting ROIs including the size and the shape which may affect the results (Shehzad et al., 2009; Van Dijk et al., 2010). ROIs are generally selected via task data or neurophysiological knowledge of researchers, which might not be applicable in some cases. Further, the time courses of pre-selected ROIs include noise. Although some strategies are applied to remove noise effect, these corrections can also affect the data (Murphy et al., 2009).

1.2.2.2. Independent component analysis (ICA)

The drawback of selecting a priori ROI for functional connectivity analysis was solved by another prominent analysis which depends more on the data itself than interference of a priori knowledge from researchers: Independent component analysis (ICA). Assuming the brain is organized into a number of functionally discrete networks, an optimal functional connectivity technique would determine the signals unique to each network. The aim of independent component analysis (ICA) is to address the problem of determining distinct components within a set of signals with

minimal a priori assumptions. Many software tools provide the tool for ICA calculation. For example, MELODIC which is built in FSL (<http://www.fmrib.ox.ac.uk/fsl>) is used to perform probabilistic ICA; GIFT can perform group ICA analysis based on SPM (<http://www.fil.ion.ucl.ac.uk/spm>); BrainVoyager 2000 (<http://www.brainvoyager.com/BrainVoyager.htm>) offers cortex-based ICA analysis; and ICA reliability can be calculated by ICASSO (Himberg et al., 2004).

As a convenient and well developed method, ICA has drawn a lot of interests among resting-state fMRI researchers. ICA can decompose the resting-state fMRI data into either spatially independent components or temporarily independent components. The spatially independent component analysis (sICA, also referred to as ICA in the following) is the more widely applied method in resting-state fMRI study due to the small number of volumes acquired in most resting-state fMRI dataset. ICA assumes that fMRI datasets are composed of mixed independent signals from a number of independent sources, and it could decompose fMRI data into several independent components (ICs) with no prior knowledge of fMRI data property. The spatial patterns of ICs represent the different brain functional networks and non-functional components, e.g. head motion and noise, which users are required to differentiate from the functionally meaningful networks. ICA is a complementary analysis to the traditional seed-based functional connectivity analysis and has been used to detect brain networks in resting-state fMRI study (Li et al., 2009).

ICA is commonly used to detect resting-state networks in the brain due to its exploratory, data-driven procedure. Kiviniemi and colleagues used ICA to analyze the fMRI data of 15 anesthetized children and found the visual network in each subject (Kiviniemi et al., 2003). Greicius and colleagues adapted ICA to derive the default mode network (DMN) in a more data-driven fashion (Greicius et al., 2004). Several resting-state networks were already detected using ICA across studies, subject groups, as well as different age groups (Van De Ven et al., 2004; Beckmann et al., 2005; De Luca et al., 2006; Fransson et al., 2007). These ICA-derive resting-state networks showed consistency across participants (Damoiseaux et al., 2006), scan sessions (Chen et al., 2008; Zuo et al., 2010b), as well as acquired data on different days (Zuo et al., 2010b). For example, Zuo and colleagues found moderate-to-high short-term (intrasession < 45min) and long-term (intersession: 5 – 16 months) test-retest

reliability for resting-state networks derived by ICA (Zuo et al., 2010b). Among many resting-state networks, the default-mode network showed particularly robust reproducibility and cross-research selection reliability (Franco et al., 2009; Meindl et al., 2010).

ICA has also been used to address clinical questions. Greicius and colleagues adopted ICA and found that patients with Alzheimer's disease (AD) showed decreased resting-state activity in the posterior cingulate and hippocampus compared to healthy controls (Greicius et al., 2004). Sorg and colleagues used ICA and also found that the default mode network (DMN) and the executive attention network demonstrated reduced network-related activity in patients at risk for AD (Sorg et al., 2007). Other studies which applied ICA to identify alteration of connectivity in clinical populations include: lateral prefrontal networks abnormality in Huntington's disease (Wolf et al., 2008), DMN deficit in mild cognitive impairment (Qi et al., 2010), DMN and sensori-motor network changes in lateral sclerosis (Mohammadi et al., 2009), contribution of subgenual cingulate cortex and thalamus abnormally increased in depression (Greicius et al., 2007), and impaired attention network in temporal lobe epilepsy (Zhang et al., 2009). In addition, connectivity analysis with ICA allowed to distinguish between patients and controls in a study on schizophrenia (Jafri et al., 2008).

In addition to identifying resting-state networks in the brain, ICA is capable of removing noise (e.g., scanner noise, physiological noise and head motion artifacts) from the fMRI dataset. After decomposing fMRI data into several ICs, there are some non-functional components which could be removed in a denoising procedure to improve quality of resting-state fMRI signal and resting-state networks' patterns. ICA-based denoising procedure is data-driven and unaffected by the temporal sampling rates (Thomas et al., 2002; Perlberg et al., 2007; De Luca et al., 2006; Tohka et al., 2008; Starck et al., 2010). For example, Thomas and colleagues found increase in BOLD contrast sensitivity values of activated voxels after adopting ICA-based noise reduction (Thomas et al., 2002).

In contrast to spatially independent component analysis (sICA), temporal ICA is not commonly used partly because this ICA requires a large number of samples to function well (Smith et al., 2012b). In a recent study, Smith and colleagues found that

multiple “temporal functional modes” of spontaneous brain activity are quite different from resting-state networks and may have greater biological interpretability. With the application of fast scanning sequences (Moeller et al., 2010; Feinberg et al., 2010) for acquiring fMRI data, temporal ICA should be able to derive ever richer and more interpretable mapping of the brain’s functions and networks in the future (Smith et al., 2012b).

Despite the promising perspective, ICA also raises some issues which one should be aware of. Firstly, the number of components in the data has to be decided before running an ICA algorithm, different numbers of components can be extracted for different individuals, further complicating the challenge (Zuo et al., 2010b). Secondly, the reproducibility of ICA is another challenging issue. Due to the ICA algorithm, the results of ICA are variable overtime. Therefore reproducibility of ICA results should be tested especially in clinical studies. Thirdly, the assumption of ICA is the independence of different sources. This assumption is wrong as fMRI BOLD signals throughout the brain are interconnected. In a recent study, Daubechies and colleagues pointed out that the ICA algorithms used in fMRI data analysis did not select for independence (Daubechies et al., 2009). Another issue of the ICA algorithm is how to select meaningful components. Generally near 50 to 100 ICs could be decomposed from resting-state fMRI data. Each independent component represents a functional network or artificial noise. Correctly selecting resting-state networks among ICs requires good background knowledge of functional neuroanatomy. Researchers have to visually check near 100 ICs in order to select plausible components which are prone to subjective errors. Some methods have been developed to select resting-state networks automatically and efficiently, e.g., template matching (Greicius et al., 2004; Seeley et al., 2009) or classification analysis to select noise ICs (De Martino et al., 2007; Tohka et al., 2008). However, a brain network template is required when using these automatically selecting methods and the selected resting-state networks could be constrained by the pattern of templates (Zuo et al., 2010b). Therefore, novel methods for automated ICA dimensionality and group-level analysis are areas of ongoing developments (Margulies et al., 2010).

1.2.2.3. Clustering

Although the data-driven approach (ICA) could solve the problem of selecting a priori

ROI for functional connectivity analysis, ICA still raises some issues which include the assumption of independence across components and how to estimate the number of components and select the meaningful networks. One approach which is used to overcome these issues is the application of clustering techniques which search for patterns in resting-state fMRI data. Clustering is generally used to classify the data into several clusters. The observations in one cluster are more similar to one another than the observations from different clusters.

Hierarchical clustering approaches are widely employed to resting-state functional connectivity data (Cordes et al., 2002; Salvador et al., 2005; Thirion et al., 2006; Cohen et al., 2008). Hierarchical clustering approaches, which are based on the single link (nearest neighbor) method to find clusters highly correlated, are appropriate similarity measures to group voxels into clusters for functional connectivity. Hierarchical clustering methods proceed by stages producing a binary cluster tree or dendrogram. At each stage in the cluster tree, objects with similar features are linked. The number of clusters at the final stage can be determined by selecting a linkage inconsistency threshold, which is one method to find the natural cluster divisions in the data set (Cordes et al., 2002). Cordes and colleagues applied hierarchical clustering to frequency-specific inter-voxel correlations and detected functional connectivity patterns which resemble known neuronal connections including sensorimotor cortex, auditory cortex, fusiform gyrus and primary visual cortex. They also found that the corresponding voxel time series in detected clusters do not show significant correlations in the respiratory or cardiac frequency band (Cordes et al., 2002). Salvador and colleagues used hierarchical clustering and multidimensional scaling of the mean partial correlation matrix, which was calculated between any two brain regions according to anatomical location, to identify six major systems in healthy volunteers - corresponding approximately to four neocortical lobes, medial temporal lobe and subcortical nuclei - that could be further decomposed into anatomically and functionally plausible subsystems (Salvador et al., 2005). Cohen and colleagues performed voxelwise hierarchical clustering on the basis of the η^2 index, which quantifies the similarity between functional connectivity patterns for every voxel pair. They showed that functional area boundaries could be reliably detected in individual subjects as well as in group data by hierarchical clustering on resting-state fMRI data.

Another commonly used clustering method is k-means clustering, which aims to partition observations into k clusters with each observation belongs to the cluster with the nearest mean (Mezer et al., 2009; Bellec et al., 2010). Mezer and colleagues used the k-means clustering approach to time-dependent measures of functional connectivity and revealed that clusters of similar BOLD fluctuations were found in the cortex but also in the white matter and sub-cortical gray matter regions (thalamus). They found high similarities between the BOLD clusters and the neuroanatomical appearance of brain regions. They also showed strong correlation between head movements and clustering quality, which suggested that non-functional contributions (head motions, the underlying microvasculature anatomy and cellular morphology) to the BOLD time series could also account for symmetric appearance of signal fluctuations (Mezer et al., 2009). Bellec and colleagues (Bellec et al., 2010) implemented k-means clustering repetitively in bootstrapping the available datasets to quantify the stability of resting-state networks. Seven resting-state networks, which included the default mode network, sensorimotor network, visual and fronto-parietal networks, were identified and exhibited a good agreement with the previous findings (Damoiseaux et al., 2006).

Van den Heuvel and colleagues used spectral clustering, which makes use of the spectrum (eigenvalues) of the similarity matrix of the data to perform dimensionality reduction before clustering in fewer dimensions, to partition whole-brain grey matter on the basis of voxelwise functional connectivity in 26 participants. They revealed seven resting-state networks which included motor/visual, auditory and attention networks and default mode network and also found these networks showed large overlap with other resting-state studies using both seed-based analysis and ICA. (Van den Heuvel et al., 2008).

The application of clustering approaches is not restricted to resting-state studies. Beckmann and colleagues applied clustering methods to magnetic resonance diffusion tractography and identified nine subregions with distinctive connectivity profiles in cingulate cortex (Beckmann et al., 2009). Palomero-Gallagher and colleagues used hierarchical clustering analysis of receptor binding according to the degree of similarity of each area's receptor architecture task activation to evaluate the validity of the four-region mode in human cingulate cortex (Palomero-Gallagher et al., 2009).

Although clustering approaches have been successfully applied to resting-state data to detect subdivisions in the brain, some limiting factors still affect its application. The most significant limiting factor is how to define the number of clusters when classifying the data due to the unknown true number of clusters. Researchers have employed different methods to find optimal cluster numbers. Given the complexity of the question, and the varying possible levels of dimensionality, it is unlikely that clustering will escape the involvement of human judgment, as users have to assess the suitability of the clustering results against known or hypothesized networks or functional subdivisions (Margulies et al., 2010).

1.2.2.4. Local methods

Both the model-driven and data-driven methods have their issues. Correlation-based techniques which have been the dominant class of methods for analyzing resting-state fMRI data rely on the selection of a region of interest (ROI) and can not fully characterize the local dynamics. The independent component analysis (ICA) needs the assumption of statistic independence. Recently, some methods which can quantify local function of brain are introduced and widely implemented in resting-state fMRI studies.

To characterize regional activity of human brain during resting state, one method is introduced: amplitude of low frequency fluctuations (ALFF). ALFF is defined as the total power within the low frequency range (for example: 0.01- 0.1 Hz) (Zang et al., 2007). For a timeseries $x(t)$ (3), ALFF is calculated as the sum of amplitudes within a specific low frequency range (4) (Zuo et al., 2010a).

$$x(t) = \sum_{k=1}^N [a_k \cos(2\pi f_k t) + b_k \sin(2\pi f_k t)] \quad (3)$$

$$ALFF = \sum_{k: f_k \in [0.01, 0.1]} \sqrt{\frac{a_k^2(f_k) + b_k^2(f_k)}{N}} \quad (4)$$

Before Zang and colleagues, low frequency fluctuations (LFF) had already been noticed in resting-state fMRI study. Biswal and colleagues found LFF to be higher in gray matter than in white matter (Biswal et al., 1995). It was also reported that low frequency oscillations (LFO) had the highest magnitude in visual regions (Kiviniemi

et al., 2003). The areas within the default mode network (Gusnard and Raichle, 2001) exhibited higher LFO amplitudes during resting state than other areas (Yang et al., 2007; Zang et al., 2007; Zou et al., 2008; Zuo et al., 2010a). Moreover, in healthy individuals, ALFF of visual cortices in eyes-open condition was significantly higher than that in eyes-closed condition (Yang et al., 2007). Zuo and colleagues revealed significant and highly reliable ranking orders of LFO amplitudes among anatomical parcellation units (Zuo et al., 2010a). Due to its easy implementation, ALFF has also been applied in clinical studies. Children with attention deficit hyperactivity disorder (ADHD) showed decreased ALFF in inferior frontal cortex and increased ALFF in anterior cingulate cortex and left sensorimotor cortex. Patients with schizophrenia showed reduced ALFF in lingual gyrus, cuneus and precuneus and increased ALFF in left parahippocampal gyrus (Hoptman et al., 2010). All these studies indicated that ALFF may be suggestive of regional spontaneous neuronal activity and can be considered as a potential bio-index in neuroimaging studies.

Some issues should be noticed: several physiological and neural factors can impact LFO amplitudes, e.g., Biswal and colleagues observed that LFO amplitudes were suppressed by hypercapnea (Biswal et al., 1997b). Some studies showed that ALFF measures are susceptible to possible artifactual findings in the vicinity of blood vessels and cerebral ventricles (Zou et al., 2008; Zuo et al., 2010a). Zou and colleagues proposed fractional amplitude of low frequency fluctuations (fALFF) to solve this problem (Zou et al., 2008). fALFF is defined as the total power within the low-frequency range (0.01 - 0.1 Hz) divided by the total power in the entire detectable frequency range, which is determined by sampling rate and duration. As a normalized index of ALFF, fALFF can provide a more specific measure of low-frequency oscillatory phenomena (Zou et al., 2008)

Another method which can also characterize the local activity of BOLD signal is regional homogeneity (ReHo). ReHo was proposed as a voxel-wise measure of the synchronization of the timecourses of neighboring voxels (Zang et al., 2004). Several resting-state fMRI studies have demonstrated brain regions that consistently show higher ReHo than others (He et al., 2004; Zang et al., 2004; Long et al., 2008), the pattern of which is consistent with the default mode network during resting-state revealed by positron emission tomography (PET) study (Gusnard and Raichle, 2001). With the advantage of having easy implementation, ReHo analysis has been used to

investigate functional modulations in the resting-state in many brain disorders including schizophrenia (Liu et al., 2006), ADHD (Cao et al., 2006), AD (He et al., 2007), remitted geriatric depression (Yuan et al., 2008), Parkinson's disease (Wu et al., 2009), epilepsy (Mankinen et al., 2010), and autism (Paakki et al., 2010). However, some parameters can affect the results of ReHo analysis: the magnitude of spatial smoothing and the size of cluster (7, 19, or 27 voxels, respectively) to be measured. Zang and colleagues suggested that a larger magnitude of spatial smoothing and a larger size of cluster yielded more significant differences between left and right finger movements (Zang et al., 2004). Zuo and colleagues pointed out that spatial smoothing of resting-state fMRI time series artificially enhances ReHo intensity and influences its reliability (Zuo et al., 2013). Therefore one should be more careful in selecting parameters when using ReHo as a complementary method to model-driven method in resting-state studies.

In summary, local methods are potentially useful in measuring local activity of human brain during rest and can be applied as complementary methods to other methods in resting state studies.

2. Study1: Tissue-Differentiation in Stroke using resting-state fMRI¹

In the following section, two resting-state fMRI methods were applied to differentiate the lesion areas, which include the infarct core and the hypoperfusion area, from healthy tissues in patients with acute ischemic stroke. Local methods which compare low frequency amplitudes of power spectrum between two hemispheres and a k-means clustering approach of functional connectivity matrix were implemented to investigate the functional damage of patients with acute ischemic stroke both in the time domain and frequency domain.

2.1 Introduction

As been introduced in Chapter 1, DWI and DSC-PWI are employed in clinical practice and in research to identify pathophysiological patterns in patients with acute ischemic stroke. DWI is thought to roughly reflect the severely damaged infarct core, while DSC-PWI reflects the area of hypoperfusion. Their volumetric difference is also termed the PWI/DWI-mismatch, and has been suggested as an MRI surrogate of the ischemic penumbra.

While in some centers PWI/DWI information is already used for clinical decision making (e.g., for the indication of fibrinolysis (Röther et al., 2002)), its clinical utility is still controversially discussed and new approaches are being sought to overcome shortcomings. This includes the application of contrast agent for PWI (Villringer et al., 1988; Rosen et al., 1990), which has potentially severe side-effects (e.g., nephrogenic systemic fibrosis), and also precludes repetitive examinations for monitoring purposes.

¹ This chapter is an expanded version of the following poster, presented at the Organization for Human Brain Mapping conference (2011): **Lv, Y.**, Margulies. D.S., Long, X., Rohr, C., Winter, B., Endres, M., Villringer, K., Fiebach, J., Villringer, A. Tissue-Differentiation in Stroke using resting-state fMRI. Poster presented at 17th Annual Meeting of the Organization for Human Brain Mapping, June 26-30, 2011, Quebec City, Canada.

Furthermore, the mismatch concept for identifying the penumbra has been challenged as being frequently inaccurate due to the lack of good quantification of perfusion at low perfusion levels and its susceptibility to alterations of the arterial input, e.g. when a carotid stenosis is present and also the difficulty in differentiating metabolically compromised brain areas from those in which blood flow is still sufficient to maintain normal cellular function and metabolism.

In searching for metabolic phenomena that may enable a novel methodology for detecting tissue state of ischemia, low-frequency fluctuations (LFF) have previously been shown to reflect the severity of cerebral ischemia (Mayevsky and Ziv, 1991), are specific to grey matter (Biswal et al., 1995; Zuo et al., 2010a), and can distinguish it from surrounding tissue and vascular signal. Previous resting-state studies have also demonstrated that brain regions can be parcellated based on unique patterns of functional connectivity in resting-state fMRI (Cohen et al., 2008; Margulies et al., 2007, 2009; Mezer et al., 2009; Bellec et al., 2010). Here we propose resting-state fMRI, which is based on the assessment of spontaneous local fluctuations of the BOLD signal, as a new approach to give pathophysiological information in the acute phase of stroke. We hypothesized that resting-state fMRI could enable differentiation of brain regions disturbed by stroke (including the infarct core and hypoperfusion areas) from healthy tissue. Furthermore, we also explored the potential for differentiating areas within the mismatch region which are truly at risk (metabolically compromised), from those which still maintain potential function.

2.2. Subjects/ Materials and Methods

2.2.1. Participants

Data was acquired from 12 patients with acute ischemic stroke one-day post-stroke onset. Informed consent was obtained from all participants prior to scanning, and all protocols were approved by the Charité Institutional Review Board EA4/026/08.

2.2.2. MR data acquisition

MR data was acquired on a Siemens Tim Trio 3 Tesla scanner located at Charité

Benjamin Franklin Hospital. The MRI scanning protocol followed the study protocol of a prospective clinical study on the value of the mismatch concept in ischemic stroke (1000+) (Hotter et al., 2009):

(1) Diffusion-weighted imaging (DWI) session: 50 axial slices, TE = 93.1 ms, TR = 7600 ms, 192x192 matrix, 2.5mm slice thickness, 90° flip angle, 14 diffusion volumes;

(2) Perfusion-weighted imaging (PWI) session: 21 axial slices, TE = 29 ms, TR = 1390 ms, 128x128 matrix, slice thickness/gap=5/0.5 mm;

(3) Fluid attenuated inversion recovery (FLAIR) session: 25 axial slices, TE = 100 ms, TR = 8000 ms, 232x256 matrix, 5mm slice thickness, 130° flip angle;

(4) Resting-state fMRI session: 34 axial slices, 64x64 matrix, voxel dimensions = 3x3x3mm+1mm gap, 90° flip angle, TE = 30 ms, TR = 2300 ms, 150 whole-brain EPI volumes.

2.2.2. Data Analysis:

2.2.2.1. Data preprocessing

Preprocessing of fMRI data was performed using both FMRIB Software Library (FSL: <http://www.fmrib.ox.ac.uk/fsl>) and Analysis of Functional NeuroImaging (AFNI: <http://afni.nimh.nih.gov/afni>) including removing first 4 volumes to allow for signal equilibration and to allow the subjects to get used to scanning noise, slice timing correction for interleaved acquisition, motion correction (by aligning each volume to the mean image using Fourier interpolation). Further image preprocessing comprised of spatial smoothing using a Gaussian kernel of FWHM 6 mm and removing the linear trend. The data were then temporally filtered using a band-pass filter (0.01-0.1 Hz).

2.2.2.2. Making mask

For all stroke patients we manually drew infarct core (from diffusion-weighted image)

and then made the mask of its symmetric areas. (Fig. 2.1)

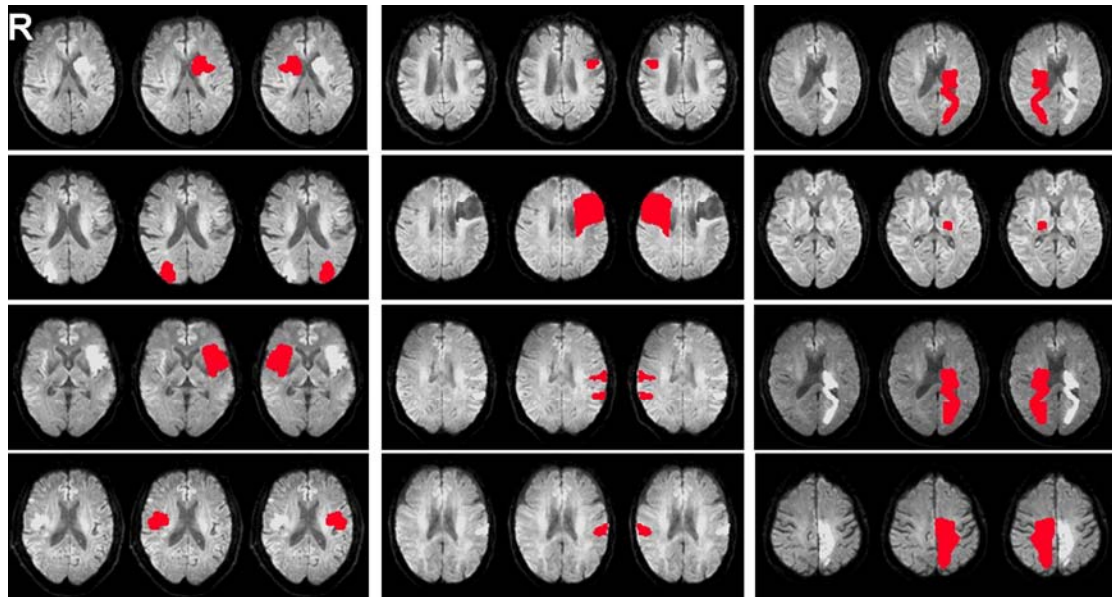


Figure 2.1: Infarct core (from DWI) and its symmetrical masks (red) of 12 stroke patients.

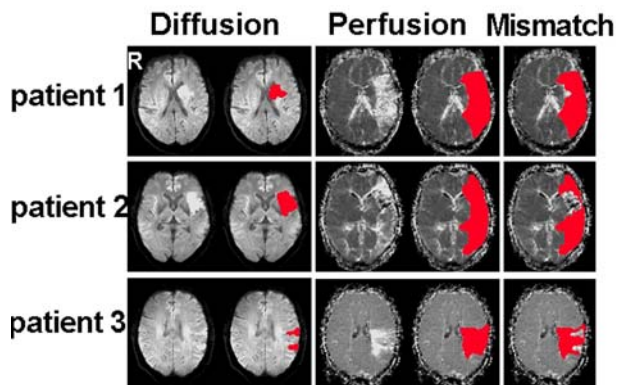


Figure 2.2: Infarct core (from DWI), hypoperfusion area (MTT map from PWI) and mismatch areas (PWI – DWI) of three patients.

For three stroke patients with mismatch areas we manually drew the masks of the affected hemisphere, the infarct core (from DWI), hypoperfusion area (mean transit time (MTT) map from PWI) and mismatch areas (PWI – DWI) respectively (Fig. 2.2)

2.2.2.3. Normalization

All the fMRI data and masks were coregistered to individual FLAIR images and subsequently spatially normalized to the Montreal Neurological Institute (MNI) template using statistical parametric mapping (SPM5 <http://www.fil.ion.ucl.ac.uk/spm>).

2.2.2.4. Analysis 1 & 2: Interhemisphere comparison of power spectrum

We extracted the average time-series of the infarct core and its symmetrical mask and calculated the power spectrum within the masks for each patient. Then a paired *t*-test was performed between power spectrum of infarct core and its contralateral healthy area.

For three stroke patients with mismatch areas, we calculated voxel-wise amplitude of power spectrum at each frequency point in the low frequency range (0.01 – 0.1Hz, 31 frequency points) and then voxel-wise interhemispheric subtraction was performed individually at homotopic voxels.

2.2.2.5. Analysis 3: Clustering

For three stroke patients with mismatch areas, the correlation matrix of time-series for each mask (affected hemisphere, hypoperfusion areas and mismatch areas) was calculated using Pearson's correlation between each pair of time-series. The correlation matrix was then classified into 2, 3, 4 and 5 clusters by k-means clustering algorithm.

2.3. Results

2.3.1. Results of Analysis 1 & 2: Interhemisphere comparison of power spectrum

When we compare the power spectrum across the whole frequency band of the infarct core with its contralateral homotopic area, the amplitude in the contralateral homotopic area is higher than that of the infarct core. Two significant differences appeared at: 0.018 Hz ($p = 0.025$) and 0.027 Hz ($p = 0.049$). (Fig 2.3)

When we perform voxel-wise interhemispheric subtraction at 31 frequency points for the three stroke patients with mismatch areas, there is one frequency point that showed maximal difference between two hemispheres for each patient, i.e. the maximal number of voxels in this frequency point have lower amplitude in the lesion area (infarct core and hypoperfusion areas) than homotopic voxels in contralateral healthy areas (Fig 2.4). Patient 1 at 0.024 Hz frequency point. Patient 2 at 0.024 Hz frequency point. Patient 3 at 0.027 Hz frequency point. Then we calculated the number of voxels in the infarct core and hypoperfused areas that have lower amplitude at this frequency point (Table 2.1).

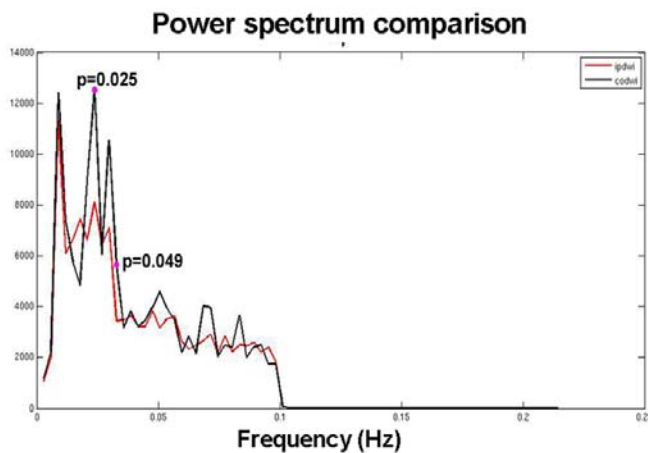


Figure 2.3: Paired *t*-test results between the power spectrum of infarct core (red) and its contralateral homotopic area (black).

Table 2.1: The number of voxels in infarct core (IC) and hypoperfusion areas (HA) that have lower amplitude than its homotopic voxels.

Number of voxels	Infarct core (IC)	Showed lower amplitude in IC	hypoperfusion area (HA)	Showed lower amplitude in HA
Patient 1	2895	2236	34382	22135
Patient 2	4581	5588	40685	31109
Patient 3	3916	3132	12373	9548

Table 2.1: The results were calculated at one frequency which has the largest number of voxels showed lower amplitude in the lesion area than the homotopic area for each patient. Patient 1 at 0.024 Hz. Patient 2 at 0.024 Hz. Patient 3 at 0.027 Hz.

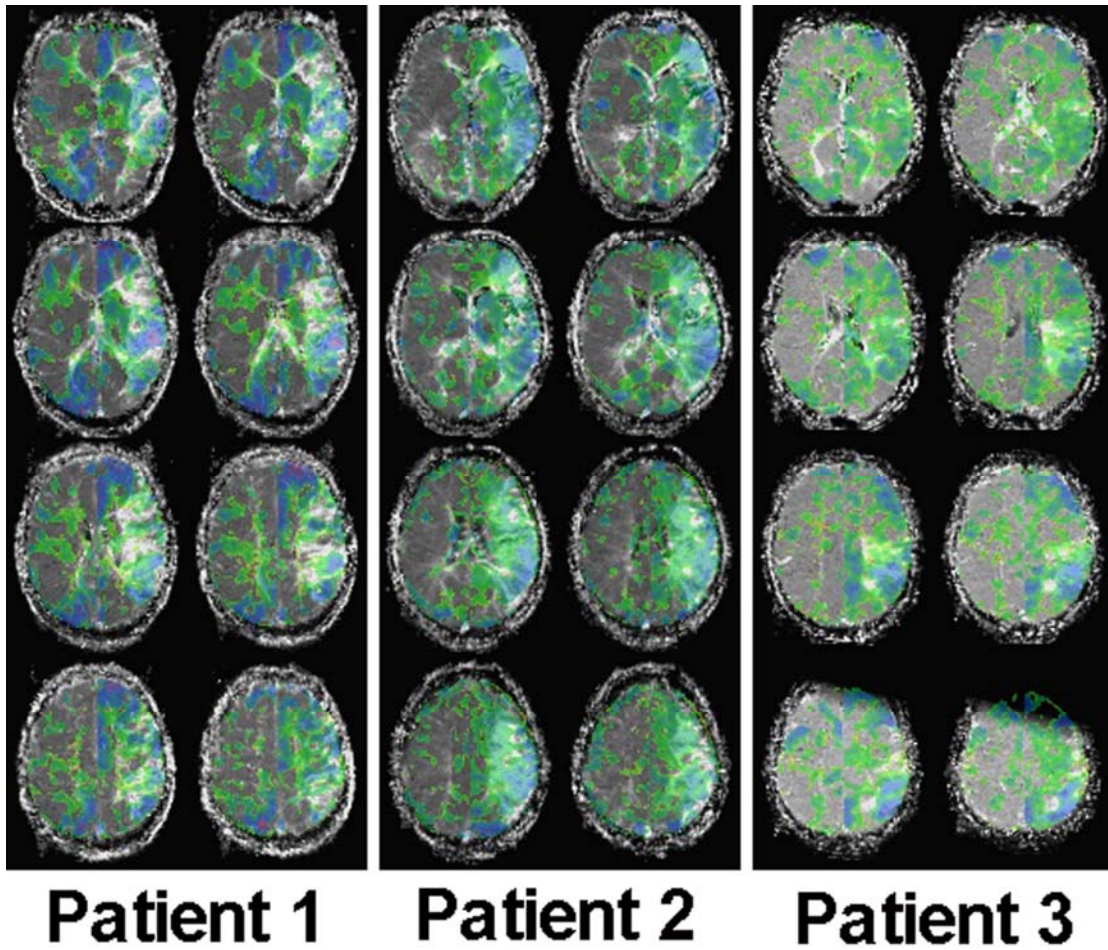


Figure 2.4: Results of voxelwise interhemispheric subtraction at one frequency which have the largest number of voxels showed lower amplitude (blue color) in the lesion area (infarct core and hypoperfusion area) than contralateral homotopic area. Patient 1 at 0.024 Hz. Patient 2 at 0.024 Hz. Patient 3 at 0.027 Hz.

2.3.2. Results of Analysis 3: Clustering

When the “affected hemisphere” was used as a mask, in all three patients, the lesion areas (infarct core and hypoperfusion area) appeared as one cluster in the three-part cluster analysis (Fig. 2.5).

When we classified the hypoperfusion areas and mismatch areas, the clustering results were highly similar. In the two-cluster results of the perfusion-disturbed areas, one cluster covered part of the infarct core which overlapped with perfusion-disturbed areas (Fig. 2.6c, yellow cluster). We hypothesized that this yellow cluster may be

functionally compromised while the red cluster represents less severely affected tissue.

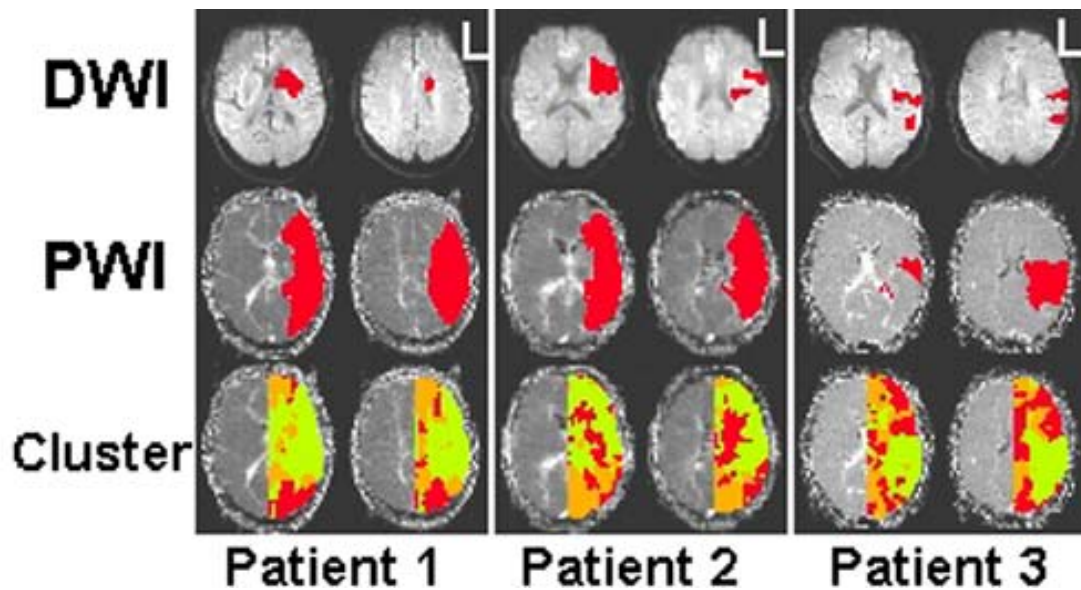


Figure 2.5: The three-cluster results of the disturbed hemisphere for three patients (Cluster). Light green cluster almost covered the disturbed areas including the infarct core (DWI) and hypoperfusion area (MTT map from PWI).

2.4. Discussion

In this study, we used resting-state fMRI to investigate the functional damages of stroke patients both in the time domain (clustering of functional connectivity matrix) and the frequency domain (interhemisphere subtraction). We wanted to differentiate brain regions affected by acute ischemic stroke from healthy tissues and differentiate areas within the mismatch region which are truly at risk (metabolically compromised) from those which still maintain potential function. The results in the frequency domain analysis, i.e. interhemisphere amplitude subtraction, showed that the lesion areas which include the infarct core and hypoperfusion area of patients with acute ischemic stroke have lower amplitudes than contralateral homotopic healthy tissues (Fig 2.4, Table 2.1). The results from clustering of the functional connectivity matrix in affected hemisphere in stroke patients showed that the lesion areas affected by the ischemic stroke (infarct core and hypoperfusion areas) appeared as one cluster (Fig 2.5). All these promising results suggest that the resting-state approach may detect the

functional damages in lesion areas of stroke patients and may serve as a useful diagnostic tool for stroke MRI to assist diagnosis and treatment of patients with acute ischemic stroke.

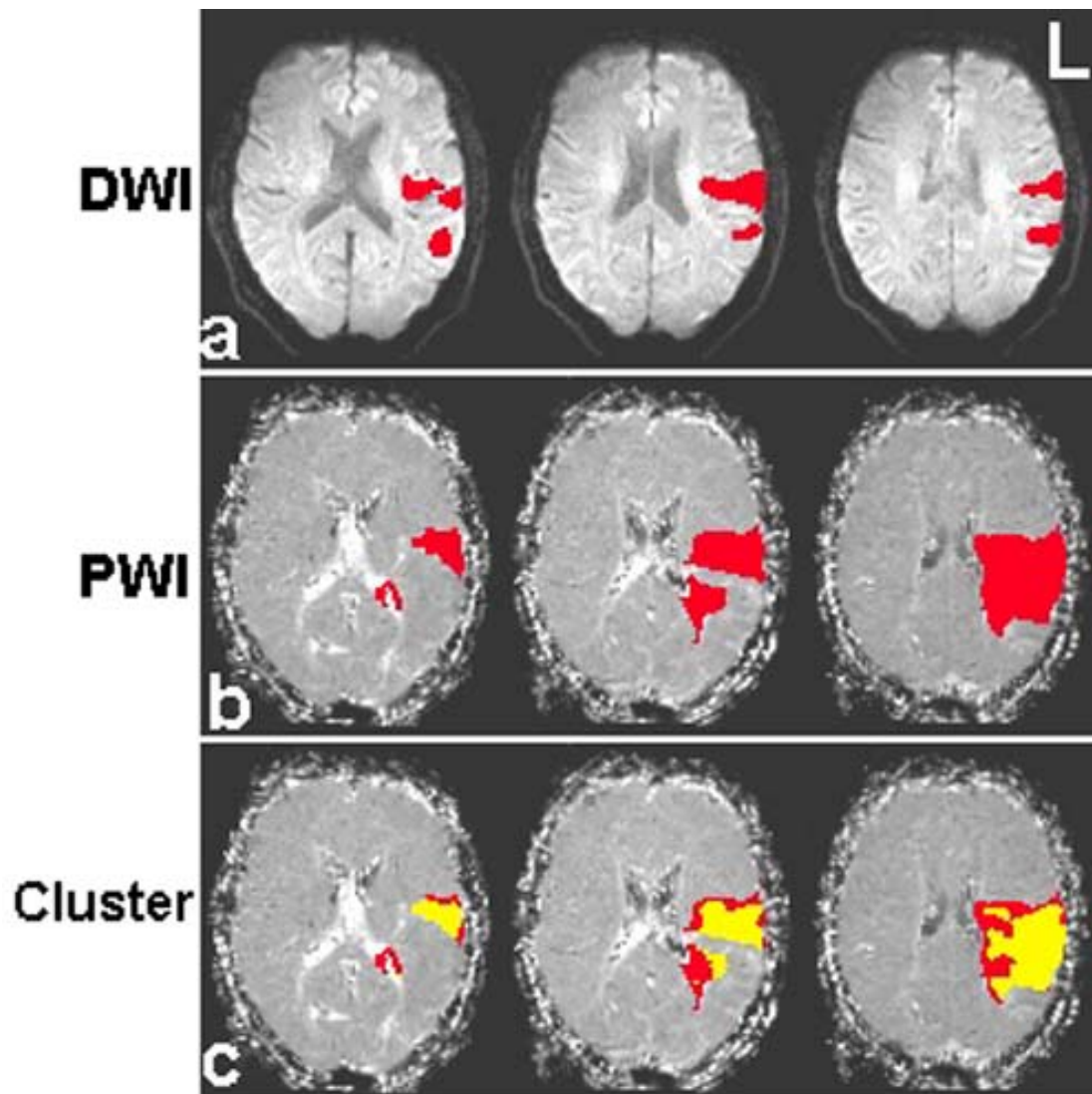


Figure 2.6: The two-cluster results of perfusion disturbed areas (c) of one patient. One cluster (c, yellow cluster) covered part of the infarct core (a) which overlapped with perfusion disturbed areas (b).

The infarct core had significant lower amplitude of the power spectrum than the contralateral homotopic area at two frequency points: 0.018 Hz ($p = 0.025$) and 0.027 Hz ($p = 0.049$) (Fig 2.3). Both frequency points are within the low-frequency band (0.01-0.1Hz) which is normally used in resting-state fMRI data preprocessing and treated as meaning oscillations. Voxel-wise interhemisphere subtraction (Fig 2.4) for three patients with mismatch areas showed the maximum difference at one frequency

for each patient (Table 2.1, Fig 2.4). These three frequency points are near the frequency (0.027 Hz) which also showed a significant difference in the infarct core (Fig 2.3). Zuo and colleagues revealed that there are symmetrical ranking orders of low-frequency oscillations (LFO) amplitudes among anatomical parcellation units across hemispheres (Zuo et al., 2010a). Our results of interhemisphere amplitude differences reflected that the ranking orders changed due to stroke. However, the reason that significant interhemisphere amplitude differences appear in a frequency near 0.027 Hz still needs to be further explored.

We found that the lesion areas (infarct core and hypoperfusion area) belonged to a single cluster when we clustered the affected hemisphere into three clusters (Fig 2.5), which revealed that clustering of resting-state fMRI data could reflect the functional difference between the lesion areas and healthy regions within the affected hemisphere. Thus clustering of resting-state data seems very promising to differentiate the lesion areas from healthy tissues.

The functional disturbance in the mismatch areas is in principle reversible. Some of these regions are truly at risk (metabolically compromised) while some still maintain potential function. When clustering hypoperfused areas and mismatch areas (Fig 2.6), the results show that one cluster (yellow) covered the infarct core, which suggests that this region is severely compromised. Our results reflect that the clustering method of resting-state fMRI data can differentiate the areas which are severely affected from the areas which still maintain function within the mismatch area.

One primary limitation is that the clustering methods took hours to parcellate the affected hemisphere of stroke patients, even with lower voxel resolution ($4 \times 4 \times 4 \text{ mm}^3$). Immediate stroke diagnosis is extremely important after stroke onset which makes it not yet feasible to apply the clustering approach in the setting of acute ischemic stroke.

In summary, in this study, we successfully used resting-state fMRI methods to differentiate the lesion areas from healthy tissues and to differentiate areas of the mismatch region that are functionally intact from apparently damaged tissue. All these results suggest that resting-state fMRI has the potential in providing useful pathophysiological information in acute ischemic stroke.

3. Study 2: Identifying the perfusion deficit in acute stroke with resting-state fMRI²

In Study 1 (Chapter 2), we successfully used two resting-state fMRI methods: (1) interhemisphere comparison of low frequency power spectrum amplitude and (2) clustering approach, to differentiate the lesion areas from healthy tissues and to differentiate areas of the mismatch region that are functionally intact from apparently damaged tissue. However, clustering consumes long time for calculation, which made it difficult to be applied in the acute phase of stroke because the therapeutic decisions must be made as quickly as possible after stroke onset. In this section, a simple resting-state method was applied to give similar pathophysiological information as DSC-PWI in the acute phase of stroke.

3.1. Introduction

In a recent study, Tong and colleagues collected resting-state fMRI (rsfMRI) and near-infrared spectroscopy (NIRS) data concurrently on six human subjects. They correlated resting-state BOLD signals with time-shifted oxyhemoglobin concentration ($\Delta[\text{HbO}]$) and found that the spatio-temporal pattern of LFOs detected by NIRS and fMRI evolves temporally through the brain in a way that resembles cerebral blood flow dynamics. These results suggested that cerebral blood flow (CBF) dynamics may be assessed with resting-state fMRI (rsfMRI) (Tong et al., 2010).

In hypoperfused areas the disturbance of CBF could affect the arrival of BOLD signal. BOLD signal in hypoperfused areas might have a time lag compared to normal tissues. In this study, we hypothesized that resting-state fMRI should contain information

² This chapter is an expanded version of the following published article: Lv, Y., Margulies, D.S., Cameron, Craddock R., Long, X., Winter. B., Gierhake, D., Endres, M., Villringer, K., Fiebach, J., Villringer. A., 2013. Identifying the perfusion deficit in acute stroke with resting-state functional magnetic resonance imaging. *Ann Neurol* 73(1), 136-140.

similar to the measures obtained from DSC-PWI, such as mean transit time (MTT) or time to peak (TTP). Here, we investigated the time delay in BOLD signal of individual voxels using rsfMRI data as a new approach to give similar pathophysiological information as DSC-PWI in the acute phase of stroke without the need for contrast agents.

3.2. Subjects/ Materials and Methods

3.2.1. Participants

Data was acquired from 17 patients with acute ischemic stroke (age = 35 – 92 years; mean = 68.4 years; 9 males and 8 females) and 38 healthy participants. 17 patients were scanned one-day post-stroke onset (2 – 30 hours (15.3 ± 9.2 hours)). Informed consent was obtained from all participants prior to scanning, and all protocols were approved by the Charité Institutional Review Board EA4/026/08. Due to severe motion confounds in 6 patients, 11 patients were included for final analysis.

3.2.2. MR data acquisition

17 patients and one healthy participant' MR data was acquired on a Siemens Tim Trio 3 Tesla scanner located at Charité Benjamin Franklin Hospital. The MRI scanning protocol followed the study protocol of a prospective clinical study on the value of the mismatch concept in ischemic stroke (1000+) (Hotter et al., 2009). For each participant the diffusion-weighted imaging (DWI) session (lasted 2 minutes and 18 seconds), the perfusion-weighted imaging (PWI) session (lasted about 2 minutes), as well as the resting-state fMRI session (lasted 5 minutes and 50 seconds) were acquired as described in “2.2.2. MR data acquisition”.

In addition to the MRI scanning session, physiological examination, the acute National Institute of Health Stroke Scale (NIHSS), also collected for each patient with acute ischemic stroke.

The resting-state fMRI sessions of another cohort of healthy participants (n = 37) were acquired in 3T Siemens Tim Trio system scanner located at Max Planck Institute for Human Cognitive and Brain Sciences in Leipzig, Germany. The parameters of resting-state fMRI session were as follows: TE = 30ms, TR = 2300ms, flip angle = 90°, matrix=64x64, voxel dimensions = 3x3x4mm, 200 whole-brain EPI volumes.

3.2.3. Data Analysis

3.2.3.1. Data preprocessing

Preprocessing of resting-state fMRI data including 17 acute ischemic stroke patients and one healthy participant was performed using both FMRIB Software Library (FSL: <http://www.fmrib.ox.ac.uk/fsl>) and Analysis of Functional NeuroImaging (AFNI: <http://afni.nimh.nih.gov/afni>) including removing first 4 volumes to allow for signal equilibration and to allow the subjects got used to scanning noise, slice timing correction for interleaved acquisition, motion correction (by aligning each volume to the mean image using Fourier interpolation). Six patients were excluded because of either large head motion (>6mm) or consistent head shaking. Further image preprocessing comprised spatial smoothing using a Gaussian kernel of FWHM 6 mm and removing the linear trend. The data were then temporally filtered using a band-pass filter (0.01-0.1 Hz).

In order to overlay resting-state fMRI data results in images with lesion areas, the DWI and the MTT map from DSC-PWI scans were coregistered to the individual's mean functional image.

For the new cohort of 37 healthy participants, the first 10 volumes of the resting-state functional images were discarded to ensure signal equilibrium and participants' adaptation to the scanning condition. Slice timing, head motion correction and spatial normalization to MNI space with 2×2×2 mm were conducted. Data were then temporally filtered using a band-pass filter (0.01-0.1 Hz).

3.2.3.2. Time-shift analysis (TSA)

We regressed the effect of head motion (using six motion parameters: three rigid body

translations and three rotations) from the resting-state fMRI data of all participants, and calculated the global average time course as reference time course. For each voxel in the brain, we extracted the time course of this voxel, and then we shifted the time course from -3 TR to 3 TR, i.e. from -6.9 s to $+6.9$ s. During the shifting, we calculated the correlation coefficients between the shifted time course of each voxel and the reference time course at each TR. For patient 3 and patient 4 (see Fig 2), which showed hypoperfusion in the MTT map from PWI scan across almost half the brain, we modified the analysis and correlated the time course of each voxel with the average time course of only the healthy hemisphere. Then for each voxel we identified the maximal correlation value and assigned the time-shift value which showed maximal correlation to the reference time course to this voxel. After the calculation, each voxel was assigned a value based on the time-shift required to the maximal correlation coefficient (Fig 3.1). So for each participant, we got a time-shift map. If the time-shift value is smaller than zero, it means the BOLD signal in this voxel has a time delay to the reference time course. If the time-shift value is larger than zero, it means the BOLD signal in this voxel precedes the reference time course.

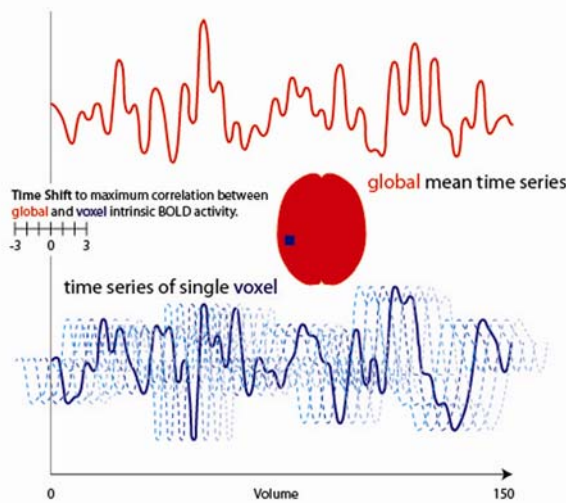


Figure 3.1: Illustration of the basic methodology for the time-shift analysis (TSA).

To test the stability of TSA result in healthy brain, we ran TSA on the new cohort of 37 healthy participants. Time-shift analysis (TSA) was not only performed for each participant to get individual time-shift map, but the group average TSA result was also calculated.

3.2.3.3. Clinical validation

Four experts in lesion delineation of the Division of Academic Neuroradiology at Charité Hospital, Berlin, traced the hypoperfusion regions (MTT) and TSA for each patient independently. Two drew the masks based on the MTT maps from PWI and the other two drew masks based on TSA delay results for each patient. Overlap was calculated using the Dice coefficient (DC), which calculates the ratio of the intersection with respect to the union of each pair of masks. In order to evaluate the similarity in mask volume, we also calculated the correlation coefficient (CC) of the volume size across the four maps across all patients. We calculated DC and CC for inter-rater MTT, inter-rater TSA, as well as between modalities respectively.

3.2.3.4. Time-shift analysis (TSA) on resting-state data with reduced volumes

The scanning time of the resting-state fMRI session was longer than the perfusion-weighted imaging (PWI) session (6 minutes vs. 2 minutes). To assess how the scanning time length might affect the TSA results we re-preprocessed and re-ran TSA on resting-state fMRI data with fewer volumes, i.e. simulating shorter acquisition times: we calculated the time-shift value on resting-state data from 30 volumes to 130 volumes in increments of 10 volumes each time. We also calculated spatial correlation of the TSA results between full scan session and decreased volumes (from 30 to 130) to check the results quality.

3.2.3.5. Correlation with clinical information

We calculated the correlation between the degree of overlap and the scanning time (hours after stroke onset), the maximal head motion as well as the acute National Institute of Health Stroke Scale (NIHSS) across patients.

3.3. Results

3.3.1. Time-shift analysis (TSA) results

A synopsis of findings in all 11 patients is provided in Table 3.1 and Figure 3.2. In all

11 patients with acute ischemic stroke TSA showed areas with a pronounced time delay to the respective mean time course (Fig 3.2). Overall, these areas corresponded to the areas of hypoperfusion as identified by MTT maps and not to the infarct cores which are reflected in the DWI image.

Table 3.1 shows the clinical information for these 11 patients with acute ischemic stroke, such as scanning time (hours for post-stroke onset), NIHSS scores in acute phase of stroke and vessel occlusion. Table 3.1 gives further information about maximal head motion, as well as the degree of overlap between modalities for each stroke patient.

Figure 3.2 shows the TSA results of 11 stroke patients and one healthy participant. For each patient with acute ischemic stroke, the upper row in the figure is the DWI image reflecting the infarct core; the middle row is the MTT from PWI session which shows the hypoperfusion area; the third row is the delay results of TSA. We used three colors to indicate the 3 delay values (-1TR red, -2TR orange, -3TR yellow). We found that the area which showed a pronounced time delay to the respective mean time course was very similar to the hypoperfusion area in perfusion MRI.

Table 3.1: Patient information

Patient #	Age / sex	Time^a (hr)	NIHSS in acute phase	Max. motion (mm)	Results of magnetic resonance angiography	Brain mask for TSA	Degree of overlap^b (DC)
1	35/ M	15	6	2.42	occlusion in M2 of MCA on the left side, and dissection of left ACI	whole	0.67
2	52/M	30	4	1.58	stenosis of the left M2 of MCA	whole	0.48
3	83/M	5	26	0.71	occlusion in M2 of MCA on the right side (multimorbid patient)	healthy hemisphere	0.40
4	52/M	10	0	0.41	95% stenosis of the left ACI	healthy hemisphere	0.63
5	68/M	9	4	2.18	posterior MCA territory on the left side with a corresponding hypoperfusion	whole	0.66
6	67/M	2	2	2.80	occlusion in P2 of PCA on the left side	whole	0.61
7	78/F	24	12	4.69	occlusion in M2 of MCA on the right side	whole	0.66
8	77/M	26	4	0.89	occlusion in P3 of PCA on the left side	whole	0.31
9	77/M	22.75	11	0.97	no occlusion	whole	0.33
10	69/M	16	17	2.29	occlusion in M1 of MCA on the right side	whole	0.70
11	82/F	9	2	5.41	occlusion in M2 of MCA on the right side	whole	0.34

^aHours post-stroke onset

^bOverlap between hypoperfusion area and TSA results as measured with Dice coefficient

DC: Dice coefficient

TSA: Time shift analysis

NIHSS = National Institute of Health Stroke Scale

MCA = Middle cerebral artery

PCA = Posterior cerebral artery

ACI = Internal carotid artery.

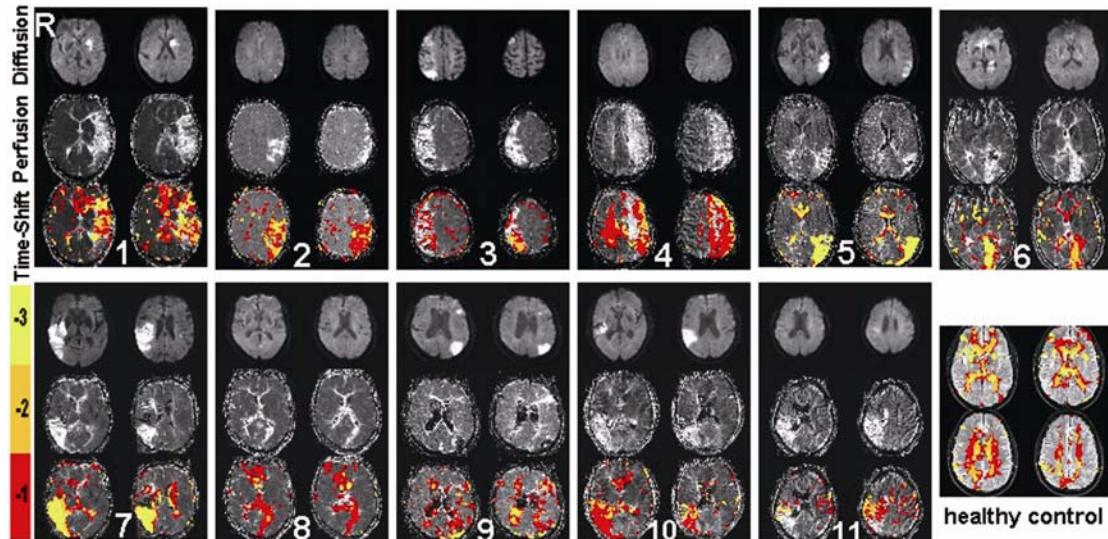


Figure 3.2: Time-shift analysis (TSA) results of 11 stroke patients and one healthy control with time-shift range from -3 TR to $+3$ TR. In 11 patients, areas affected by the ischemic stroke (hypoperfused) show a pronounced time delay to the global mean time course. In one healthy control, the time lagged areas were approximately symmetrically distributed within ventricular areas. -1, -2, -3 in color bar indicates -1 TR, -2 TR, -3 TR time shift.

Detailed time-shift analysis (TSA) results for each patient with acute ischemic stroke:

Both the pronounced mismatches in patient 2, patient 6, patient 8 (Fig 3.3) and the smaller mismatch in patient 5, patient 7, patient 9 as well as patient 10 (Fig 3.4) are clearly apparent: the areas which showed time delays to global mean corresponded to the areas of hypoperfusion as identified by MTT maps and not to the infarct cores reflected in DWI.

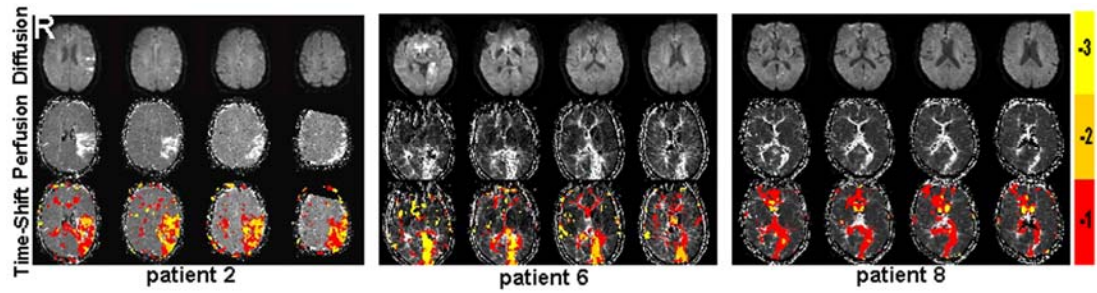


Figure 3.3: Detailed time-shift analysis (TSA) results of 3 stroke patients (2, 6, 8) with a time-shift range from -3 TR to +3 TR. In these 3 patients who have large mismatch areas, the areas which showed time delays to global mean corresponded to the areas of hypoperfusion as identified by MTT maps and not to the infarct cores which are reflected in DWI. -1, -2, -3 in color bar indicates -1 TR, -2 TR, -3 TR time shift.

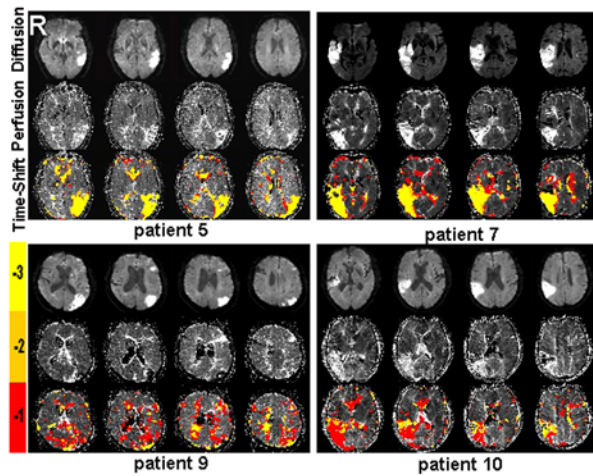


Figure 3.4: Detailed time-shift analysis (TSA) results of 4 stroke patients (5, 7, 9 and 10) with time-shift range from -3 TR to +3 TR. In these 4 patients who have small mismatch areas, the areas which showed time delays to global mean corresponded to the areas of hypoperfusion as identified by MTT maps and not to the infarct cores which are reflected in DWI. -1, -2, -3 in color bar indicates -1 TR, -2 TR, -3 TR time shift.

In patient 1 (Fig 3.5), in addition to the TSA delay results which overlap with MTT maps from PWI, the TSA map also showed a time delay in medial prefrontal areas which probably is caused by head motion during the scanning. The maximal head motion of this patient was 2.42 mm.

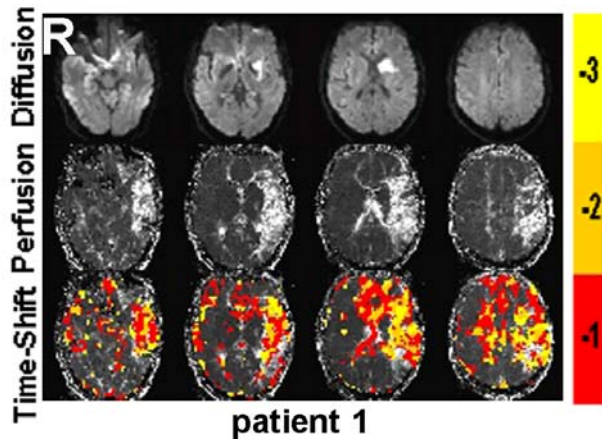


Figure 3.5: Detailed time-shift analysis (TSA) results of stroke patient 1 with time-shift range from -3 TR to +3 TR. In this patient there is also a time delay in medial prefrontal areas which probably is caused by head motion. -1, -2, -3 in color bar indicates -1 TR, -2 TR, -3 TR time shift.

An additional methodological consideration is illustrated in patient 3 and patient 4 (Fig 3.6), who suffered very large infarctions covering the MCA territory shown in the middle row of Figure 3.6: the hypoperfusion area in the MTT map covers almost half of the brain. As the whole brain mask would have been too “contaminated” by signal from hypoperfused tissue, we chose to use the average time course from only the “healthy” hemisphere as the reference time series. The result from patient 4 shows a high degree of overlap (DC=0.67) with areas specific to the perfusion deficit within the affected hemisphere, while patient 3 shows a low degree of overlap (DC=0.40), likely caused by the large infarct core (DWI).

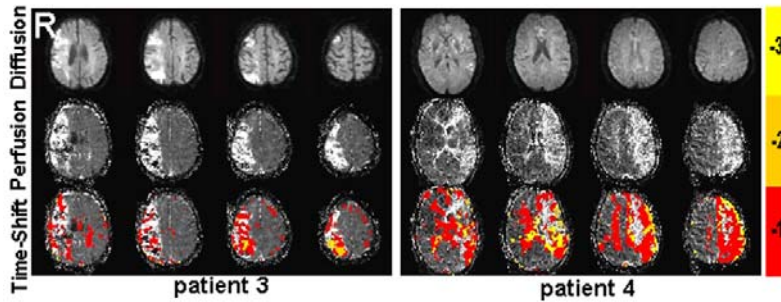


Figure 3.6: Detailed time-shift analysis (TSA) results of 2 stroke patients (patient 3 and patient 4) with time-shift range from -3 TR to +3 TR. These two patients have large hypoperfusion area which occupied almost the whole hemisphere, the average time course from only the “healthy” hemisphere was used as reference time course in TSA analysis. -1, -2, -3 in color bar indicates -1 TR, -2 TR, -3 TR time shift.

Large head motion in patient 11 likely caused a low degree of overlap ($DC = 0.34$). The maximal head motion displacement of this patient was 5.4 mm and there were many spikes in the head motion curve of this patient (Fig 3.7). The results in this patient indicated that the head motion seriously affected the TSA results.

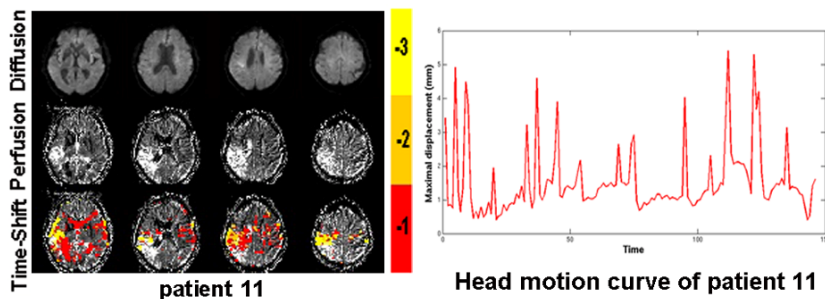


Figure 3.7: Detailed time-shift analysis (TSA) results of stroke patient 11 with time-shift range from -3 TR to +3 TR. Head motion curve of this patient is given in the right. -1, -2, -3 in color bar indicates -1 TR, -2 TR, -3 TR time shift.

When we calculated the time delay of each voxel’s time course in the healthy brain, the areas showing a clear time delay to the global mean were symmetrically distributed and located largely within the ventricles (Fig 3.2, Fig 3.8), while smaller time delays were identified in adjacent white matter.



Figure 3.8: Detailed time-shift analysis (TSA) results of one healthy control with time-shift range from -3 TR to +3 TR. The time lagged areas were approximately symmetrically distributed within ventricular areas. -1, -2, -3 in color bar indicates -1 TR, -2 TR, -3 TR time shift.

To test the stability of TSA result in healthy brain, we ran TSA on another cohort of 37 healthy participants. The group average TSA result showed a similar pattern as presented in the healthy control in Figure 3.8: the areas showing a clear time delay to the global mean were symmetrically distributed and located largely within the ventricles, while smaller time delays were identified in adjacent white matter (Fig 3.9).

3.3.2. Clinical validation results:

In order to validate the TSA approach for clinical application purposes, four experts in stroke imaging manually outlined lesions on MTT and TSA maps independently. We calculated both the CC of the number of voxels included in the lesions between the masks across patients, and the DC for calculating the degree of overlap in each individual patient, which were then averaged: Inter-rater MTT: CC=0.95, DC=0.66; inter-rater TSA: CC=0.93, DC=0.70. The between modalities results were: CC=0.79, DC=0.53.

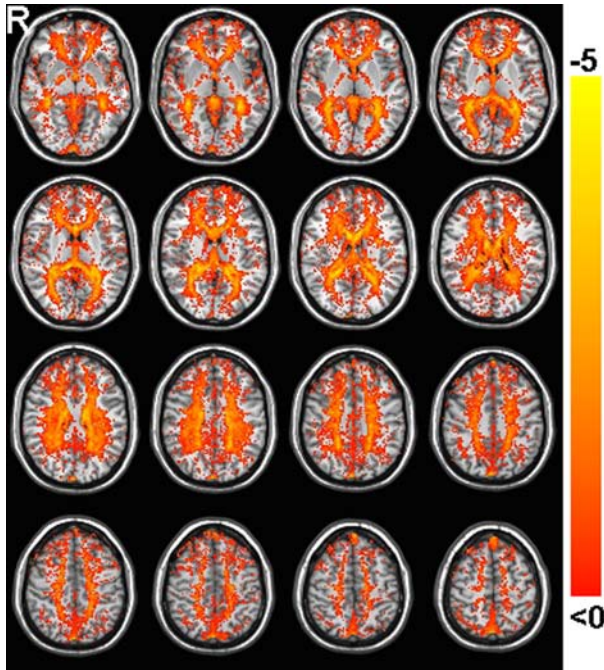


Figure 3.9: Group average of time-shift analysis (TSA) results of 37 healthy controls with time-shift range from -3 TR to +3 TR, the time lagged areas were approximately symmetrically distributed within ventricular areas.

3.3.3. Time-shift analysis (TSA) results on resting-state data with reduced volumes:

As the resting-state fMRI session (6 min) was longer than standard PWI scans (2 min), we tested the impact of decreasing the scan length on the TSA results. Decreasing the scan length used for the analysis (in increments of 10 volumes), we found that 184 seconds (with 80 volumes left) still showed similar results to the full scan session (Fig 3.10). Some patients even showed similar results just with 50 volumes remaining (115 seconds). We also calculated spatial correlation of the TSA results between full scan session and decreased volumes (from 30 to 130), which was monotonically increasing (Fig 3.11). In future data acquisition, such parameters may prove valuable to making practical decisions about acquisition length in clinical settings.

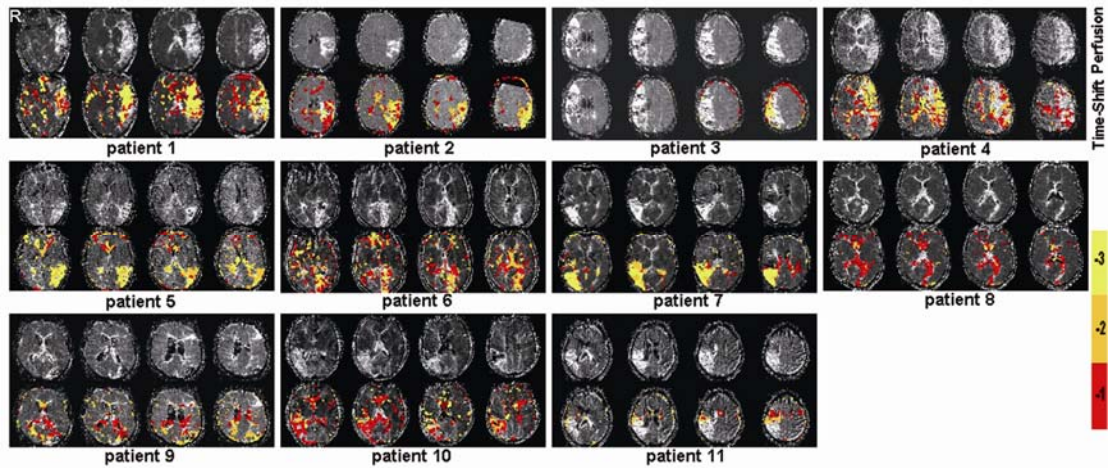


Figure 3.10: Time-shift analysis (TSA) results of 80 resting-state volumes for each stroke patient with time-shift range from -3 TR to +3 TR. In all 11 patients, areas affected by the ischemic stroke show a pronounced time delay to the global mean time course. The affected area is similar to the area of hypoperfusion. The color bar refers to: -1 TR, -2 TR, -3 TR time shift.

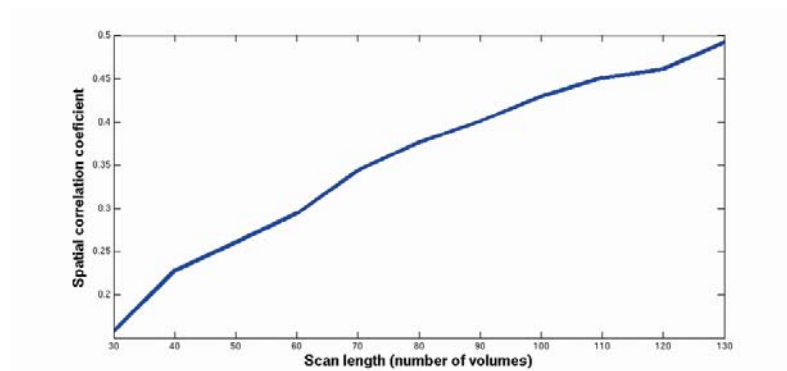


Figure 3.11: Spatial correlation of the TSA results between full scan session and decreased volumes (from 30 to 130).

3.3.4. Other results:

For 11 patients with acute ischemic stroke we also calculated the MTT (mean transit time) and TTP (time to peak) difference between the ipsilateral hypoperfusion area and contralateral healthy regions (Table 3.2): TTP range from 0.4 to 15.7s (6.1 ± 4.5 s), MTT range from 0.4s to 4.3s (2.3 ± 1.2 s).

Table 3.2: The average difference between the ipsilateral hypoperfusion area and contralateral healthy regions for MTT and TTP values in 11 stroke patients

Patient #	TTP delay^a (s) (within # TR)	MTT delay^b (s) (within # TR)
1	3.1 (2 TR)	1.3 (1 TR)
2	2.7 (2 TR)	3.6 (2 TR)
3	15.7 (7 TR)	2.3 (1 TR)
4	0.4 (1 TR)	0.4 (1 TR)
5	3.0 (2 TR)	0.8 (1 TR)
6	10.1 (5 TR)	2.7 (2 TR)
7	5.4 (3 TR)	2.1 (1 TR)
8	2.4 (2 TR)	1.8 (1 TR)
9	6.6 (3 TR)	4.3 (2 TR)
10	9.8 (5 TR)	3.8 (2 TR)
11	8.2 (4 TR)	2.3 (1 TR)

^aThe average TTP difference between ipsilateral hypoperfusion area and contralateral healthy regions.

^bThe average MTT difference between ipsilateral hypoperfusion area and contralateral healthy regions.

TTP: Time to peak

MTT: Mean transit time

TR: Repetition time, in this study, TR = 2.3s

To assess whether the scanning time (hours after stroke onset), the maximal head motion or the acute National Institute of Health Stroke Scale (NIHSS) affect the degree of overlap between lesion on mean transit time (MTT) map and TSA results, we calculated the correlation between these indices. There was no correlation between post-stroke scanning time and degree of overlap ($r = -0.23$, $p = 0.50$), acute NIHSS and degree of overlap ($r = -0.06$, $p = 0.86$), maximal head motion and degree of overlap ($r = 0.15$, $p = 0.65$).

3.4. Discussion

In this study, we successfully used rsfMRI to identify hypoperfused areas in acute stroke. We suggest that an assessment of time delays of the spontaneous low frequency fluctuations of the BOLD signal may provide comparable information to parameters of contrast based perfusion MRI such as MTT (Ostergaard et al., 1996), and thus serve as a useful diagnostic tool for stroke MRI without the need for the application of a contrast agent. We show that TSA maps corresponded to the PWI-MTT defined areas, and not to the DWI lesion.

Previous DSC-PWI studies have reported delays of MTT in stroke in the range of 0-8s (Schellinger et al., 2006), with a difference between the affected and non-affected hemisphere of 0.4-5.6s (1.3 ± 1.9 s) (Mihara et al., 2003). In our study, we also calculated the average difference between the ipsilateral hypoperfusion area and contralateral healthy regions for MTT and TTP values in 11 acute ischemic stroke patients. The MTT delays ranged from 0.4s to 4.3s (2.3 ± 1.2 s) (Table 3.2), suggesting that the time shift range which we employed for TSA (± 6.9 s) in this study was reasonable.

The primary limiting factor for clinical application of the current approach is its sensitivity to head motion. Six patients had to be excluded from further analysis due to motion artifacts. We applied regressing out the head motion effect and ICA-based denoising approaches to make our data viable for each patient. However, the ICA-based approaches did not improve our results considerably. From the TSA delay results of patient 11 one can notice the serious head motion effect to TSA, as shown in Figure 3.7. The maximal head motion displacement of this patient was 5.4 mm and there were many spikes in the head motion curve. Still the time delay result looked plausible in this patient (Fig 3.7). Thus, to be clinically viable, it would be valuable to find effective ways to manage head motion, such as prospective motion correction during scanning and reducing scanning time of data acquisition, i.e. the scanning time can be reduced to ~3 minutes as shown in Figure 3.10: when only 80 volumes were scanned TSA delay results of 11 patients still showed similar results to the full scan session (150 volumes). In future studies, real-time motion estimation or real-time TSA assessment could facilitate decisions regarding repeating or prolonging the

measurement - viable clinical options, as no contrast agent application is necessary.

The other issue of the TSA method is that with low temporal resolution (TR=2300ms) we can hardly compare the time delay value (-1, -2, -3 TR) to MTT delay value. Further improvement of the method may be achieved by acquiring resting-state fMRI data at a higher temporal resolution. The whole brain resting-state fMRI data could be acquired within 400ms or 300ms (Moeller et al., 2010; Feinberg et al, 2010), thus we could increase the time-shift numbers when TSA is applied on such fast resting-state fMRI data. With more time-shift delay values for voxels in the brain, the time-shift delay values should be closer to the MTT delay values, which is likely to further improve the precision of hypoperfusion assessment.

Another limiting factor in this study is that MRI data was acquired from patients with ischemic stroke within a wide time range, i.e., 2-30 hours (15.3 ± 9.2 h) after stroke onset. Since the important clinical decisions (e.g. thrombolysis) should be made within 3-9 hours (only 4 patients in our study), the TSA approach should clearly be validated for this time window before any clinical decisions be based upon it.

The current findings suggest TSA as a promising new approach to assessing hemodynamics in stroke. Although it is just a first step, this straightforward measure provides strong evidence that there is key information about tissue perfusion that can be extracted from resting-state fMRI data. The other interesting non-invasive approach for perfusion imaging, arterial spin labeling (ASL), so far has been hampered by poor signal-to-noise ratio in situations of long transit times (Petersen et al., 2006). In a recent study, Bokkers and colleagues used an improved pseudocontinuous labeling scheme in ASL, which has increased the signal-to-noise ratio because it has a higher labeling efficiency and enables the combined use of the body transmit coil with the multidetector coils, to detect perfusion deficits in patients with acute ischemic stroke and showed that ASL can depict large perfusion and perfusion-diffusion mismatches in correspondence with DSC-PWI. However, ASL still missed 7 out of 39 perfusion lesions (Bokkers et al., 2012). Hence given the hitherto unsatisfactory “performance” of ASL in the clinical situation the development of new non invasive alternatives is highly desirable. In our study, perfusion lesions were detected in all 11 patients by the time shift analysis.

In summary, we believe that resting-state fMRI appears to be sensitive for detecting

severe hypoperfusion area in acute stroke, and holds promise to provide a valuable alternative to current techniques, opening a new place for resting-state fMRI in acute stroke diagnostics.

4. General discussion and outlook

In this thesis, I have investigated the application of resting-state fMRI methods in acute ischemic stroke. In Chapter 2, we successfully applied a clustering method that parcellated brain regions based on unique patterns of functional connectivity using spontaneous brain activity in resting-state fMRI to differentiate the lesion areas (infarct core plus hypoperfusion area) from healthy tissues and to differentiate areas of the mismatch regions that are functionally unique from apparently damaged tissues. In Chapter 3, perfusion lesions were successfully detected in all 11 patients by time-shift analysis (TSA). We suggest that an assessment of time delays of the spontaneous low frequency fluctuations of the BOLD signal may provide comparable information to parameters of DSC-PWI such as MTT and thus serve as a useful diagnostic tool for stroke MRI without the need for the application of a contrast agent.

Compared with the clustering method, the time-shift analysis (TSA) approach showed more promising prospects owing to its simple implementation, less time-consuming computation, as well as better results. Aside from the contrast agent usage, there are advantages of resting-state fMRI: rsfMRI enables the possibility of conducting multiple scanning sessions without potential harm to the patient. If the patient has moved during contrast agent injection, the information is lost. With rsfMRI one simply repeats the data acquisition. Although this is not yet a final evidence of the utility of TSA for resting-state fMRI data, it is rather a first step towards that goal. Our study is the very first approach using resting-state fMRI and with newer pulse sequences at much higher temporal resolution (Feinberg et al., 2010; Moeller et al., 2010), we envision much improved performance in the near future.

However, there remain some limiting factors for clinical application of the TSA approach such as: (1) with low temporal resolution ($TR=2300ms$) we can hardly compare the time delay values to the mean transit time (MTT) delay values from DSC-PWI; (2) head motion; (3) white matter and cerebral spinal fluid (CSF) effect. In the future, our research will focus on optimizing the time-shift analysis (TSA) method as outlined subsequently.

4.1. Optimization of time-shift analysis (TSA) method

4.1.1. Fast scan sequence for resting-state fMRI scanning

With the development of fast scan sequences for BOLD contrast (Moeller et al., 2010; Feinberg et al., 2010), resting-state fMRI whole brain dataset could be acquired at much higher temporal resolution. Feinberg and colleagues used the multiplexed-EPI pulse sequence which combines two forms of multiplexing: temporal multiplexing (m) utilizing simultaneous echo refocused (SIR) EPI and spatial multiplexing (n) with multibanded radio frequency pulses (MB) to achieve $m \times n$ images in an EPI echo train instead of the normal single image. They successfully reduced EPI scan time to achieve a TR of 400 ms for whole brain fMRI at a 3 Tesla MRI scanner (Feinberg et al., 2010). By using this new sequence, we could acquire whole brain resting-state fMRI data in shorter time. During TSA with the same time range we can increase the time shift numbers and thus there will be more time-shift delay values for voxels in the brain. Thus the TSA time delay values should be closer to the MTT delay values or to the real delay values of cerebral blood flow in the hypoperfusion area.

This fast scan sequence has been installed at the Max Planck Institute for Human Cognitive and Brain Sciences. We have acquired resting-state fMRI dataset to test its quality. I will show some results of one testing experiment in the following part.

In this testing scanning, we acquired the data from one healthy participant (24 years old, female) with five resting state fMRI sessions, the parameters were as follows:

(1) First resting-state fMRI session: TR = 2300 ms, 150 whole-brain EPI volumes, 90° flip angle (FA);

(2) Second resting-state fMRI session: TR = 1150 ms, 300 whole-brain EPI volumes, 90° flip angle;

(3) Third resting-state fMRI session: TR = 766 ms, 450 whole-brain EPI volumes, 90° flip angle;

(4) Fourth resting-state fMRI session: TR = 460 ms, 750 whole-brain EPI volumes, 90° flip angle;

(5) Fifth resting-state fMRI session: TR = 460 ms, 750 whole-brain EPI volumes, 45° flip angle;

Other parameters were the same for five sessions: 30 axial slices, 64x64 matrix, voxel dimensions = 3x3x3mm+1mm gap, TE = 30 ms

We preprocessed the five resting-state fMRI session in the same way as described in “3.2.3.1. Data preprocessing”. Then we performed time-shift analysis (TSA), functional connectivity analysis with a seed region of interest (ROI) located in the posterior cingulate cortex (PCC). We also assessed the signal-to-noise ratio (SNR) to test the quality of resting-state fMRI data with different temporal resolution.

The SNR in the “short TR session” was lower than in the “long TR session”, while the functional connectivity map showed no difference among these sessions. The TSA time delay results are given in Figure 4.1. For each session, the time range was the same (-6.9s ~ 6.9s) when running TSA. The time-shift numbers were increased with TR decreasing, e.g. time-shift ranged from -3TR to 3TR with TR = 2300ms while from -15TR to 15TR with TR = 460ms. In all five resting-state fMRI sessions, the areas showing a clear time delay to the global mean were symmetrically distributed and located largely within the ventricles, while smaller time delays were identified in adjacent white matter (Fig 4.1). These results were very similar to the results showed in Chapter 3: Figure 3.8, Figure 3.9. As we expected, there were more time-shift delay values in the maps based on the “short TR session” than the one based on the “long TR session.

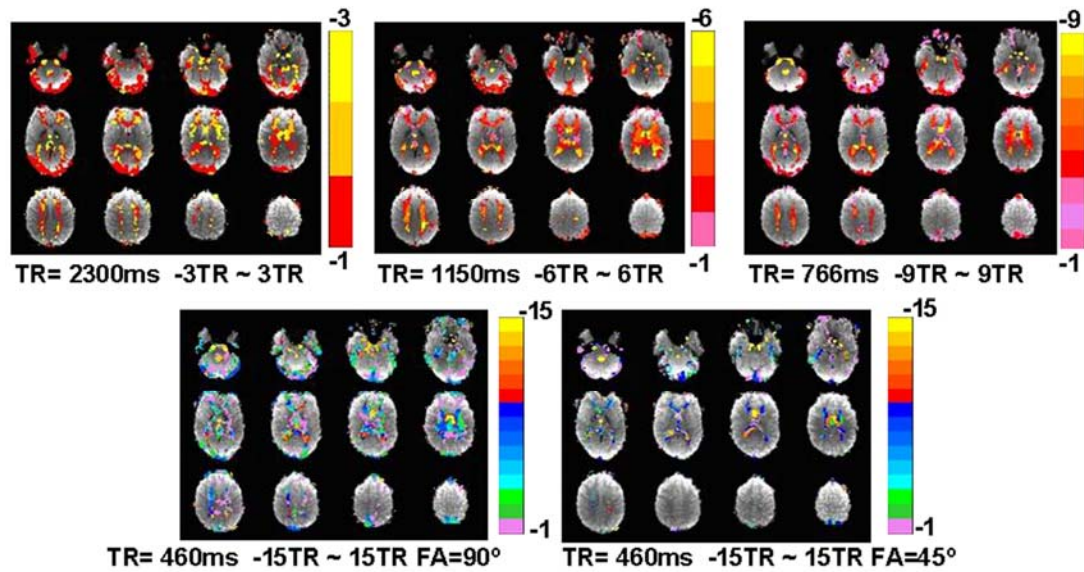


Figure 4.1 Time-shift analysis (TSA) results for five resting-state fMRI sessions with different TR. The time range were the same (-6.9s ~ 6.9s), while time-shift numbers were different across sessions. The time lagged areas were approximately symmetrically distributed within ventricular areas. The values of the color bar indicates time shift values (e.g. In TR=766ms, -9 means the time shift value was -9TR).

4.1.2. Other improvements for TSA optimization

The primary limiting factor for the clinical application of the TSA approach seems to be the susceptibility to head motion. As we discussed in Chapter 3, real-time motion correction during scanning and reducing scanning time would be effective ways to solve this problem. In the future, we can reduce the scanning time to 3 minutes and observe the head motion during scanning, which may improve the TSA time delay results.

Secondly, we could optimize the reference time course for TSA. For example, we could choose the average time course of a homotopic region contralateral to the hyperperfused area in the healthy hemisphere as the reference time course, which may be better for assessing the time delay values in the hypoperfusion area.

Further potential improvements of the method include removing the effect of white matter and CSF. As shown in Figure 3.2 (Chapter 3), the area showed a time delay to

the reference time course not just in the hypoperfusion area but also in the ventricular area and in the white matter. In future research, we may segment the anatomical image, extract time courses from white matter and CSF and then regress out the effect of white matter and CSF from the BOLD signal. We should further more validate our approach for a 3-9 hours time window which is relevant for therapeutic decisions.

Another aspect of future work may be the combination of resting-state fMRI and 3D arterial spin labeling (ASL) fMRI technique. The other interesting non-invasive approach for perfusion imaging, arterial spin labeling (ASL), so far has been hampered by poor signal to noise in situations of long transit times. In a recent study which applied ASL to reflect the perfusion deficits of acute ischemic stroke patients, ASL still missed 7 out of 39 perfusion lesions (Bokkers et al., 2012). But the authors also pointed out that the perfusion deficit volume in 7 missed patients was very small and the 3D whole brain ASL may resolve this problem. ASL can also provide perfusion information of healthy participants which we can use to compare with TSA time delay results in healthy controls. The combination of resting-state fMRI and 3D ASL may further improve the accuracy of perfusion deficit assessment.

4.2. Heart beat acts as bolus for measuring perfusion shifts in BOLD-fMRI

As we introduced in Chapter 1, in dynamic susceptibility contrast-enhanced perfusion-weighted imaging (DSC-PWI), the contrast agent passage causes the signal fall in brain tissue which increases with the perfused cerebral blood volume (CBV). In our study, we found that the cerebral blood perfusion information may be included in the resting-state fMRI BOLD signal. We propose to use the heart beat as bolus for measuring perfusion shifts in BOLD-fMRI in future studies.

BOLD fMRI signal includes information such as the response to heart beat, the response to respiration, other low frequency oscillations, vascular response to neural activity etc. If we can extract the BOLD signal response to the heart beat, after each heart beat we could calculate the time delay of the BOLD signal response at every voxel in the brain. The time delay value in the hypoperfusion area should be lagged from normal tissues. Therefore, by simultaneously recording the electrocardiogram

(ECG) and resting state fMRI BOLD signal we may assess the perfusion deficit more accurately.

4.3. Other thoughts for future research

Following are some ideas for future investigation:

(1) Longitudinal study. We can acquire the MRI data not only in the acute ischemic phase, but also one day, two days, one week, one month, 90 days and half a year after stroke onset to monitor the perfusion deficit and help the recovery of patients.

(2) Real-time processing of MRI data. It took only ten minutes or even less to complete preprocessing and the TSA on resting-state fMRI dataset. Therefore, it seems possible to perform the analysis during MRI scanning and provide the time delay results of BOLD signal and ASL perfusion data immediately after scanning.

(3) In studies on an animal model of stroke, we can precisely control the time of stroke onset, position of vessel blockage, as well as the degree of damage, which will further improve our methods and help clinical diagnosis and treatment of acute ischemic stroke.

(4) Application of resting-state fMRI methods in other brain diseases. For example, the study of perfusion disturbance caused by cerebral hemorrhage, traumatic brain injury or brain tumor.

Summary

Dissertation zur Erlangung des akademischen Grades

Dr. rer. med.

Application of resting-state fMRI methods to acute ischemic stroke

eingereicht von: Yating Lv

angefertigt am Max-Planck-Institut für Kognitions- und Neurowissenschaften

betreut von Prof. Dr. Arno Villringer und Dr. Daniel S. Margulies

Juni 2013

As the second leading cause of death and major cause of disability in the world (Donnan et al., 2008; Mathers et al., 2009), stroke is the rapid loss of brain function due to disturbance in the blood supply to the brain. Stroke can cause permanent neurological damage, complications, and death. Acute ischemic stroke is caused by the blockage of a blood vessel in the brain. Therapeutic decisions must be made quickly after stroke onset, where minutes can make the difference between benefit and harm to the patient. The rapid diagnosis is crucial for patient outcome after stroke onset. Diffusion weighted imaging (DWI) and dynamic susceptibility contrast-enhanced (DSC) perfusion-weighted imaging (PWI) are commonly employed in clinical practice and in research to give pathophysiological information for patients with acute ischemic stroke (Sorensen et al., 1996; Wardlaw, 2010; Merino and Warach, 2010; Dani et al., 2011). DWI is thought to roughly reflect the severely damaged infarct core due to cytotoxic edema which is caused by the breakdown of sodium-potassium pumps, while DSC-PWI reflects the area of hypoperfusion due to hemodynamic compromise in the brain. The volumetric difference between DWI and DSC-PWI is termed the PWI/DWI-mismatch, and has been suggested as an MRI surrogate of the ischemic penumbra (Karonen et al., 1999; Schlaug et al., 1999). The cerebral blood flow (CBF) damage in the mismatch area is potentially reversible. If

normal CBF is restored in time, the ischemic damage in the penumbra can be minimized, otherwise long-term hypoperfusion in penumbra will eventually lead to infarction. Therefore the ischemic penumbra is regarded as the prime target for any treatment approach after acute ischemic stroke onset.

However, the mismatch concept for identifying the penumbra has been challenged as being frequently inaccurate due to the lack of good quantification of perfusion at low perfusion levels and its susceptibility to alterations of the arterial input. Due to the application of a contrast agent, which, though effective to induce a transient change in MRI signal due to magnetic susceptibility effects (Villringer et al., 1988), has potentially severe side-effects (e.g., nephrogenic systemic fibrosis), the DSC-PWI precludes repetitive examinations for monitoring purposes. New approaches are being sought to overcome this shortcoming.

Resting-state functional magnetic resonance imaging (rsfMRI) is a noninvasive imaging technique which does not require contrast agent application and is of relatively low cost, while still maintaining high temporal resolution. Therefore, resting-state fMRI is increasingly applied to research questions regarding brain disorders (Li et al., 2002; Greicius et al., 2004). The BOLD (blood oxygen-level dependent) signal used in rsfMRI reflects oxygen metabolism as well as hemodynamics (Tong et al., 2010).

The aim of this thesis was to use resting-state fMRI as a new approach to give similar information as DSC-PWI. Specifically, we aim to apply the resting-state fMRI approach to differentiate the lesion areas from healthy tissues in patients with acute ischemic stroke. This thesis comprises two studies:

In the first study (see Chapter 2), two resting-state fMRI methods, local methods which compare low frequency amplitudes between two hemispheres and a k-means clustering approach, were applied to investigate the functional damage of patients with acute ischemic stroke both in the time domain and frequency domain. In the second study (see Chapter 3), time-shift analysis (TSA), which assesses time delays of the spontaneous low frequency fluctuations of the resting-state BOLD signal, was applied to give similar pathophysiological information as DSC-PWI in the acute phase of stroke.

More specifically, with these two studies we have found that:

1. The lesion areas which include the infarct core and the hypoperfusion area of patients with acute ischemic stroke had lower amplitudes than contralateral homotopic healthy tissues in the low frequency range. (see Fig 2.3 and Fig 2.4).
2. Using a k-means clustering approach on resting-state fMRI data, the lesion areas (infarct core and hypoperfusion area) belonged to a single cluster, which reflected that the clustering method could differentiate the lesion areas from healthy tissues (see Fig 2.5). The results suggest that k-means clustering is a promising approach to be developed further.
3. Using time-shift analysis (TSA), areas which showed a pronounced time delay to the respective mean time course were very similar to the hypoperfusion area in patients with acute ischemic stroke, while the areas showing a clear time delay to the global mean were symmetrically distributed and located largely within the ventricles and white matter in healthy controls (see Fig 3.2). The results suggest that an assessment of time delays of the spontaneous low frequency fluctuations of the BOLD signal may provide comparable information to parameters of DSC-PWI such as mean transit time (MTT), and thus serve as a useful diagnostic tool for stroke MRI without the need for the application of a contrast agent.

Lesion areas (infarct core and hypoperfusion area) had significant lower amplitude of power spectrum near 0.027 Hz than contralateral homotopic area. However, the reasons why significant interhemisphere amplitude differences appear in a frequency near 0.027 Hz still needs to be further explored.

Even though we could differentiate lesion areas from healthy tissues using clustering methods on resting-state data for patients with acute ischemic stroke, one primary limitation is that clustering methods took hours to parcellate the affected hemisphere of stroke patients, even with lower voxel resolution ($4 \times 4 \times 4 \text{ mm}^3$). Immediate stroke diagnosis is extremely important after stroke onset which makes it not yet feasible to apply the clustering approach in the setting of acute ischemic stroke.

Compared with the clustering method, the time-shift analysis (TSA) approach, with simple implementation, less time-consuming computation, as well as better results,

showed more promising prospects for clinical practice. However, the primary limiting factor for clinical application of the TSA method was the susceptibility to head motion, e.g. six patients were excluded from further analysis in our study due to motion artifacts. Thus, to be clinically viable, it would be valuable to find effective ways to overcome head motion, such as prospective motion correction during scanning and reducing scanning time of data acquisition. Real-time motion estimation could facilitate decisions regarding repeating or prolonging the measurement—viable clinical options, as no contrast agent application is necessary.

The other limiting factor of the TSA method is that with low temporal resolution (TR=2300ms) we can hardly compare the time delay values to mean transit time (MTT) values from DSC-PWI. Further improvement of the method may be achieved by acquiring resting-state fMRI data at a higher temporal resolution. The whole brain resting-state fMRI data could be acquired within 400ms or 300ms (Moeller et al., 2010; Feinberg et al, 2010), allowing to increase the time-shift numbers. With more time-shift delay values for voxels in the brain, the time-shift delay values will be closer to the MTT delay values, which is likely to further improve the precision of hypoperfusion assessment.

In summary, resting-state fMRI appears to be sensitive for detecting severe hypoperfusion areas in acute ischemic stroke, and holds promise to provide a valuable alternative to current techniques, opening a new place for rsfMRI in acute stroke diagnostics.

Article and presentation included in this thesis:

Lv, Y., Margulies, D.S., Cameron, Craddock R., Long, X., Winter. B., Gierhake, D., Endres, M., Villringer, K., Fiebach, J., Villringer. A., 2013. Identifying the perfusion deficit in acute stroke with resting-state functional magnetic resonance imaging. *Ann Neurol* 73(1), 136-140.

Lv, Y., Margulies. D.S., Long, X., Rohr, C., Winter, B., Endres, M., Villringer, K., Fiebach, J., Villringer, A. Tissue-Differentiation in Stroke using resting-state fMRI. Poster presented at 17th Annual Meeting of the Organization for Human Brain Mapping, June 26-30, 2011, Quebec City, Canada.

References

Achard, S., Salvador, R., Whitcher, B., Suckling, J., Bullmore, E., 2006. A resilient, low-frequency, small-world human brain functional network with highly connected association cortical hubs. *J Neurosci* 26(1), 63-72.

Alsop, D.C., Detre, J.A., 1996. Reduced transit-time sensitivity in noninvasive magnetic resonance imaging of human cerebral blood flow. *J Cereb Blood Flow Metab* 16(6), 1236-1249.

Astrup, J., Siesjö, B.K., Symon, L., 1981. Thresholds in cerebral ischemia - the ischemic penumbra. *Stroke* 12(6), 723-725.

Beckmann, C.F., DeLuca, M., Devlin, J.T., Smith, S.M., 2005. Investigations into resting-state connectivity using independent component analysis. *Philos Trans R Soc Lond B Biol Sci* 360(1457), 1001-1013.

Beckmann, M., Johansen-Berg, H., Rushworth, M.F., 2009. Connectivity-based parcellation of human cingulate cortex and its relation to functional specialization. *J Neurosci* 29(4), 1175-1190.

Bellec, P., Rosa-Neto, P., Lyttelton, O.C., Benali, H., Evans, A.C., 2010. Multi-level bootstrap analysis of stable clusters in resting-state fmri. *Neuroimage* 51, 1126-1139.

Biswal, B., Yetkin, F.Z., Haughton, V.M., Hyde, J.S., 1995. Functional connectivity in the motor cortex of resting human brain using echo-planar MRI. *Magn Reson Med* 34(4), 537-541.

Biswal, B., Hudetz, A.G., Yetkin, F.Z., Haughton, V.M., Hyde, J.S., 1997a. Hypercapnia reversibly suppresses low-frequency fluctuations in the human motor cortex during rest using echo-planar MRI. *J Cereb Blood Flow Metab* 17, 301-308.

Biswal, B.B., Van Kylen, J., Hyde, J.S., 1997b. Simultaneous assessment of flow and BOLD signals in resting-state functional connectivity maps. *NMR Biomed* 10(4-5), 165-170.

Bokkers, R.P., Hernandez, D.A., Merino, J.G., Mirasol, R.V., van Osch, M.J., Hendrikse, J., Warach, S., Latour, L.L., 2012. Whole-Brain Arterial Spin Labeling Perfusion MRI in Patients With Acute Stroke. *Stroke* 43(5), 1290-1294.

Borogovac, A., Asllani, I., 2012. Arterial Spin Labeling (ASL) fMRI: advantages, theoretical constraints, and experimental challenges in neurosciences. *Int J Biomed Imaging* 2012, 818456.

Cao, Q., Zang, Y., Sun, L., Sui, M., Long, X., Zou, Q., Wang, Y., 2006. Abnormal neural activity in children with attention deficit hyperactivity disorder: a resting-state functional magnetic resonance imaging study. *Neuroreport* 17(10), 1033-1036.

Chen, S., Ross, T., Zhan, W., Myers, C., Chuang, K., Heishman, S., Stein, E., Yang, Y., 2008. Group independent component analysis reveals consistent resting-state networks across multiple sessions. *Brain Res* 1239 (6), 141-151.

Cohen, A.L., Fair, D.A., Dosenbach, N.U., Miezin, F.M., Dierker, D., Van Essen, D.C., Schlaggar, B.L., Petersen, S.E., 2008. Defining functional areas in individual human brains using resting functional connectivity MRI. *Neuroimage* 41(1), 45-57.

Cordes, D., Haughton, V.M., Arfanakis, K., Wendt, G.J., Turski, P.A., Moritz, C.H., Quigley, M.A., Meyerand, M.E., 2000. Mapping functionally related regions of brain with functional connectivity MR imaging. *AJNR Am J Neuroradiol* 21(9), 1636-1644.

Cordes, D., Haughton, V.M., Arfanakis, K., Carew, J.D., Turski, P.A., Moritz, C.H., Quigley, M.A., Meyerand, M.E., 2001. Frequencies contributing to functional connectivity in the cerebral cortex in "resting-state" data. *AJNR Am J Neuroradiol* 22(7), 1326-1333.

Cordes, D., Haughton, V., Carew, J.D., Arfanakis, K., Maravilla, K., 2002. Hierarchical clustering to measure connectivity in fmri resting-state data. *Magn Reson Imaging* 20(4), 305-317.

Damoiseaux, J.S., Rombouts, S.A., Barkhof, F., Scheltens, P., Stam, C.J., Smith, S.M., Beckmann, C.F., 2006. Consistent resting-state networks across healthy subjects. *Proc Natl Acad Sci U S A* 103, 13848-13853.

Dani, K.A., Thomas, R.G., Chappell, F.M., Shuler, K., MacLeod, M.J., Muir, K.W., Wardlaw, J.M., 2011. Computed tomography and magnetic resonance perfusion imaging in ischemic stroke: Definitions and thresholds. *Ann Neurol* 70(3), 384-401.

Daubechies, I., Roussos, E., Takerkart, S., Benharrosh, M., Golden, C., D'Ardenne, K., Richter, W., Cohen, J.D., Haxby, J., 2009. Independent component analysis for brain fmri does not select for independence. *Proc Natl Acad Sci U S A* 106(26), 10415-10422.

De Luca, M., Beckmann, C.F., De Stefano, N., Matthews, P.M., Smith, S.M., 2006. fMRI resting state networks define distinct modes of long-distance interactions in the human brain. *Neuroimage* 29, 1359-1367.

De Martino, F., Gentile, F., Esposito, F., Balsi, M., Di Salle, F., Goebel, R., Formisano, E., 2007. Classification of fMRI independent components using IC-fingerprints and support vector machine classifiers. *Neuroimage* 34(1), 177-194.

Diestel, R., 2005. *Graph Theory*, volume 173 of Graduate Texts in Mathematics. Springer, 3rd edition.

Di Martino, A., Scheres, A., Margulies, D.S., Kelly, A.M., Uddin, L.Q., Shehzad, Z., Biswal, B., Walters, J.R., Castellanos, F.X., Milham, M.P., 2008. Functional connectivity of human striatum: a resting state fmri study. *Cereb Cortex* 18(12), 2735-2747.

Donnan, G.A., Fisher, M., Macleod, M., Davis, S.M., 2008. Stroke. *Lancet* 371(9624), 1612-1623.

Feinberg, D.A., Moeller, S., Smith, S.M., Auerbach, E., Ramanna, S., Gunther, M., Glasser, M.F., Miller, K.L., Ugurbil, K., Yacoub, E., 2010. Multiplexed echo planar imaging for sub-second whole brain FMRI and fast diffusion imaging. *PLoS One* 5(12), e15710.

Franco, A., Pritchard, A., Calhoun, V., Mayer, A., 2009. Interrater and intermethod reliability of default mode network selection. *Hum Brain Mapp* 30(7), 2293-2303.

Fransson, P., Skiold, B., Horsch, S., Nordell, A., Blennow, M., Lagercrantz, H., Aden, U., 2007. Resting-state networks in the infant brain. *Proc Natl Acad Sci U S A* 104, 15531-15536.

Greicius, M.D., Krasnow, B., Reiss, A.L., Menon, V., 2003. Functional connectivity in the resting brain: a network analysis of the default mode hypothesis. *Proc Natl Acad Sci U S A* 100(1), 253-258

Greicius, M.D., Srivastava, G., Reiss, A.L., Menon, V., 2004. Default-mode network activity distinguishes Alzheimer's disease from healthy aging: evidence from functional MRI. *Proc Natl Acad Sci U S A* 101(13), 4637-4642.

Greicius, M.D., Flores, B.H., Menon, V., Glover, G.H., Solvason, H.B., Kenna, H., Reiss, A.L., Schatzberg, A.F., 2007. Resting-state functional connectivity in major depression: abnormally increased contributions from subgenual cingulate cortex and thalamus. *Biol Psychiatry* 62(5), 429-437.

Gusnard, D.A., Raichle, M.E., 2001. Searching for a baseline: functional imaging and the resting human brain. *Nat Rev Neurosci* 2, 685-694.

Hacke, W., Warach, S., 2000. Diffusion-weighted MRI as an evolving standard of care in acute stroke. *Neurology* 54(8),1548-1549.

Hampson, M., Peterson, B.S., Skudlarski, P., Gatenby, J.C., Gore, J.C., 2002. Detection of functional connectivity using temporal correlations in MR images. *Hum Brain Mapp* 15(4), 247-262.

Hampson, M., Olson, I.R., Leung, H.C., Skudlarski, P., Gore, J.C., 2004. Changes in functional connectivity of human MT/V5 with visual motion input. *Neuroreport* 15(8), 1315-1319.

He, Y., Zang, Y., Jiang, T., Liang, M., Gong, G., 2004. Detecting functional connectivity of the cerebellum using low frequency fluctuations (LFFs). In C. Barillot, D. R. Haynor, & P. Hellier (Eds.), *Medical image computing and computer-assisted intervention MICCAI*, 907-915. Berlin, Heidelberg, St. Malo, France: Springer.

He, Y., Wang, L., Zang, Y., Tian, L., Zhang, X., Li, K., 2007. Regional coherence changes in the early stages of Alzheimer's disease: A combined structural and resting-state functional MRI study. *Neuroimage* 35, 488-500.

Himberg, J., Hyvärinen, A., Esposito, F., 2004. Validating the independent components of neuroimaging time series via clustering and visualization. *Neuroimage* 22(3), 1214-1222.

Hoptman, M.J., Zuo, X.N., Butler, P.D., Javitt, D.C., D'Angelo, D., Mauro, C.J., Milham, M.P., 2010. Amplitude of low-frequency oscillations in schizophrenia: A resting state fMRI study. *Schizophr Res* 117(1), 13-20

Hotter, B., Pittl, S., Ebinger, M., Oepen, G., Jegzentis, K., Kudo, K., Rozanski, M., Schmidt, W.U., Brunecker, P., Xu, C., Martus, P., Endres, M., Jungehülsing, G.J., Villringer, A., Fiebich, J.B., 2009. Prospective study on the mismatch concept in acute stroke patients within the first 24 h after symptom onset - 1000Plus study. *BMC Neurol* 9, 60.

Jafri, M.J., Pearlson, G.D., Stevens, M., Calhoun, V.D., 2008. A method for functional network connectivity among spatially independent resting-state components in schizophrenia. *Neuroimage* 39(4), 1666-1681.

Kahn, I., Andrews-Hanna, J.R., Vincent, J.L., Snyder, A.Z., Buckner, R.L., 2008. Distinct cortical anatomy linked to subregions of the medial temporal lobe revealed by intrinsic functional connectivity. *J Neurophysiol* 100(1), 129-139.

Karonen, J.O., Vanninen, R.L., Liu, Y., Ostergaard, L., Kuikka, J.T., Nuutinen, J., Vanninen, E.J., Partanen, P.L., Vainio, P.A., Korhonen, K., Perkiö, J., Roivainen, R., Sivenius, J., Aronen, H.J., 1999. Combined diffusion and perfusion MRI with correlation to single-photon emission CT in acute ischemic stroke. Ischemic penumbra predicts infarct growth. *Stroke* 30(8), 1583-1590.

Kiviniemi, V., Jauhiainen, J., Tervonen, O., Pääkkö, E., Oikarinen, J., Vainionpää, V., Rantala, H., Biswal, B., 2000. Slow vasomotor fluctuation in fMRI of anesthetized child brain. *Magn Reson Med* 44(3), 373-378.

Kiviniemi, V., Kantola, J.H., Jauhiainen, J., Hyvärinen, A., Tervonen, O., 2003. Independent component analysis of non-deterministic fMRI signal sources. *Neuroimage* 19, 253-260.

Kiviniemi, V., Kantola, J.H., Jauhiainen, J., Tervonen, O., 2004. Comparison of methods for detecting nondeterministic BOLD fluctuation in fMRI. *Magn Reson Imaging* 22(2), 197-203.

Krienen, F.M., Buckner, R.L., 2009. Segregated fronto-cerebellar circuits revealed by intrinsic functional connectivity. *Cereb Cortex* 19(10), 2485-2497.

Kwong, K.K., Belliveau, J.W., Chesler, D.A., Goldberg, I.E., Weisskoff, R.M., Poncelet, B.P., Kennedy, D.N., Hoppel, B.E., Cohen, M.S., Turner, R., 1992. Dynamic magnetic resonance imaging of human brain activity during primary sensory stimulation. *Proc Natl Acad Sci U S A* 89(12), 5675-5679.

Latchaw, R.E., Alberts, M.J., Lev, M.H., Connors, J.J., Harbaugh, R.E., Higashida, R.T., Hobson, R., Kidwell, C.S., Koroshetz, W.J., Mathews, V., Villablanca, P., Warach, S., Walters, B., 2009. Recommendations for imaging of acute ischemic stroke: a scientific statement from the American heart association. *Stroke* 40(11), 3646-3678.

Leopold, D.A., Murayama, Y., Logothetis, N.K., 2003. Very slow activity fluctuations in monkey visual cortex: implications for functional brain imaging. *Cereb Cortex* 13(4), 422-433.

Le Bihan, D., Breton, E., Lallemand, D., Grenier, P., Cabanis, E., Laval-Jeantet, M., 1986. MR imaging of intravoxel incoherent motions: application to diffusion and perfusion in neurologic disorders. *Radiology* 161, 401-407.

Le Bihan, D., Breton, E., Lallemand, D., Grenier, P., Cabanis, E., Laval-Jeantet, M., 1988. Separation of diffusion and perfusion in intravoxel incoherent motion MR imaging. *Radiology* 168, 497-505.

Le Bihan, D., Mangin, J.F., Poupon, C., Clark, C.A., Pappata, S., Molko, N., Chabriat, H., 2001. Diffusion tensor imaging: concepts and applications. *J Magn Reson Imaging* 13(4), 534-546.

Li, K., Guo, L., Nie, J., Li, G., Liu, T., 2009. Review of methods for functional brain connectivity detection using fMRI. *Comput Med Imaging Graph* 33(2), 131-139.

Li, S.J., Li, Z., Wu, G., Zhang, M.J., Franczak, M., Antuono, P.G., 2002. Alzheimer Disease: evaluation of a functional MR imaging index as a marker. *Radiology* 225(1), 253-259.

Liu, H., Liu, Z., Liang, M., Hao, Y., Tan, L., Kuang, F., Yi, Y., Xu, L., Jiang, T.Z., 2006. Decreased regional homogeneity in schizophrenia: A resting state functional magnetic resonance imaging study. *Neuroreport* 17, 19-22.

Logothetis, N.K., Pauls, J., Augath, M., Trinath, T., Oeltermann, A., 2001. Neurophysiological investigation of the basis of the fMRI signal. *Nature* 412(6843), 150-157.

Long, X.Y., Zuo, X.N., Kiviniemi, V., Yang, Y., Zou, Q.H., Zhu, C.Z., Jiang, T.Z., Yang, H., Gong, Q.Y., Wang, L., Li, K.C., Xie, S., Zang, Y.F., 2008. Default mode network as revealed with multiple methods for resting-state functional MRI analysis. *J Neurosci Methods* 171(2), 349-55.

Lowe, M.J., Mock, B.J., Sorenson, J.A., 1998. Functional connectivity in single and multislice echoplanar imaging using resting-state fluctuations. *Neuroimage* 7(2), 119-132.

Lowe, M.J., Dzemidzic, M., Lurito, J.T., Mathews, V.P., Phillips, M.D., 2000. Correlations in low-frequency BOLD fluctuations reflect cortico-cortical connections. *Neuroimage* 12(5), 582-587.

Mankinen, K., Long, X.Y., Paakki, J.J., Harila, M., Rytty, S., Tervonen, O., Nikkinen, J., Starck, T., Remes, J., Rantala, H., Zang, Y.F., Kiviniemi, V., 2010. Alterations in regional homogeneity of baseline brain activity in pediatric temporal lobe epilepsy. *Brain Res* 1373, 221-229.

Mansfield, P., 1977. Multi-planar image formation using NMR spin echos. *J Phys C10*, L55-L58.

Mansfield, P., 1984. Real-time echo-planar imaging by NMR. *Br Med Bull* 40, 187-190.

Margulies, D.S., Kelly, A.M., Uddin, L.Q., Biswal, B.B., Castellanos, F.X., Milham, M.P., 2007. Mapping the functional connectivity of anterior cingulate cortex. *Neuroimage* 37(2), 579-588.

Margulies, D.S., Vincent, J.L., Kelly, C., Lohmann, G., Uddin, L.Q., Biswal, B.B., Villringer, A., Castellanos, F.X., Milham, M.P., Petrides, M., 2009. Precuneus shares intrinsic functional architecture in humans and monkeys. *Proc Natl Acad Sci U S A* 106(47), 20069-20074.

Margulies, D.S., Böttger, J., Long, X., Lv, Y., Kelly, C., Schäfer, A., Goldhahn, D., Abbushi, A., Milham, M.P., Lohmann, G., Villringer, A., 2010. Resting developments: a review of fMRI post-processing methodologies for spontaneous brain activity. *MAGMA* 23(5-6), 289-307.

Mathers, C.D., Boerma, T., Ma Fat, D., 2009. Global and regional causes of death. *Br Med Bull* 92, 7-32.

Mayevsky, A., Ziv, I., 1991. Oscillations of cortical oxidative metabolism and microcirculation in the ischaemic brain. *Neurological research* 13(1), 39-47.

McCormick, D.A., 1999. Spontaneous activity: signal or noise? *Science* 285(5427), 541-543.

Meindl, T., Teipel, S., Elmouden, R., Mueller, S., Koch, W., Dietrich, O., Coates, U., Reiser, M., Glaser, C., 2010. Test-retest reproducibility of the default-mode network in healthy individuals. *Hum Brain Mapp* 31(2), 237-246.

Merino, J.G., Warach, S., 2010. Imaging of acute stroke. *Nat Rev Neurol*. 6(10), 560-571.

Mezer, A., Yovel, Y., Pasternak, O., Gorfine, T., Assaf, Y., 2009. Cluster analysis of resting-state fMRI time series. *Neuroimage* 45(4), 1117-1125.

Mihara, F., Kuwabara, Y., Tanaka, A., Yoshiura, T., Sasaki, M., Yoshida, T., Masuda, K., Matsushima, T., 2003. Reliability of mean transit time obtained using perfusion-weighted MR imaging; comparison with positron emission tomography. *Magn Reson Imaging* 21(1), 33-39.

Moeller, S., Yacoub, E., Olman, C.A., Auerbach, E., Strupp, J., Harel, N., Uğurbil, K., 2010. Multiband multislice GE-EPI at 7 tesla, with 16-fold acceleration using partial parallel imaging with application to high spatial and temporal whole-brain fMRI. *Magn Reson Med* 63,1144-1153.

Mohammadi, B., Kollwe, K., Samii, A., Krampfl, K., Dengler, R., Münte, T., 2009. Changes of resting state brain networks in amyotrophic lateral sclerosis. *Exp Neurol* 217(1), 147-153.

Moseley, M.E., Cohen, Y., Mintorovitch, J., Chileuitt, L., Shimizu, H., Kucharczyk, J., Wendland, M.F., Weinstein, P.R., 1990. Early detection of regional cerebral ischemia in cats: comparison of diffusion- and T2-weighted MRI and spectroscopy. *Magn Reson Med* 14, 330-346.

Murphy, K., Birn, R., Handwerker, D., Jones, T., Bandettini, P., 2009. The impact of global signal regression on resting state correlations: are anti-correlated networks introduced? *NeuroImage* 44 (3), 893-905.

Ogawa, S., Lee, T.M., Kay, A.R., Tank, D.W., 1990. Brain magnetic resonance imaging with contrast dependent on blood oxygenation. *Proc Natl Acad Sci U S A* 87(24), 9868-9872.

Ostergaard, L., Weisskoff, R.M., Chesler, D.A., Gyldensted, C., Rosen, B.R., 1996. High resolution measurement of cerebral blood flow using intravascular tracer bolus passages. Part I: Mathematical approach and statistical analysis. *Magn Reson Med* 36(5), 715-725.

Paakki, J.J., Rahko, J., Long, X., Moilanen, I., Tervonen, O., Nikkinen, J., Starck, T., Remes, J., Tuula, H., Haapsamo, H., Jussila, K., Kuusikko-Gauffin, S., Mattila, M.L., Zang, Y., Kiviniemi, V., 2010. Alterations in Regional Homogeneity of Resting-State Brain Activity in Autism Spectrum Disorders. *Brain Res* 1321, 169-179

- Palomero-Gallagher, N., Vogt, B.A., Schleicher, A., Mayberg, H.S., Zilles, K., 2009. Receptor architecture of human cingulate cortex: evaluation of the four-region neurobiological model. *Hum Brain Mapp* 30(8), 2336-2355.
- Pelled, G., Goelman, G., 2004. Different physiological MRI noise between cortical layers. *Magn Reson Med* 52(4), 913-916.
- Perlberg, V., Bellec, P., Anton, J.-L., Péligrini-Issac, M., Doyon, J., Benali, H., 2007. CORSICA: correction of structured noise in fMRI by automatic identification of ICA components. *Magn Reson Imaging* 25(1), 35-46.
- Petersen, E.T., Zimine, I., Ho, Y.C., Golay, X., 2006. Non-invasive measurement of perfusion: a critical review of arterial spin labelling techniques. *Br J Radiol* 79(944), 688-701.
- Qi, Z., Wu, X., Wang, Z., Zhang, N., Dong, H., Yao, L., Li, K., 2010. Impairment and compensation coexist in amnesic MCI default mode network. *Neuroimage* 50(1):48-55.
- Raichle, M.E., MacLeod, A.M., Snyder, A.Z., Powers, W.J., Gusnard, D.A., Shulman, G.L., 2001. A default mode of brain function. *Proc Natl Acad Sci U S A* 98(2), 676-682.
- Rosen, B.R., Belliveau, J.W., Vevea, J.M., Brady, T.J., 1990. Perfusion imaging with NMR contrast agents. *Magn Reson Med* 14(2), 249-265.
- Röther, J., Schellinger, P.D., Gass, A., Siebler, M., Villringer, A., Fiebach, J.B., Fiehler, J., Jansen, O., Kucinski, T., Schoder, V., Szabo, K., Junge-Hülsing, G.J., Hennerici, M., Zeumer, H., Sartor, K., Weiller, C., Hacke, W., 2002. Effect of intravenous thrombolysis on MRI parameters and functional outcome in acute stroke <6 hours. *Stroke* 33(10), 2438-2445.
- Roy, A.K., Shehzad, Z., Margulies, D.S., Kelly, A.M., Uddin, L.Q., Gotimer, K., Biswal, B.B., Castellanos, F.X., Milham, M.P., 2009. Functional connectivity of the human amygdala using resting state fmri. *Neuroimage* 45, 614-626.

Salvador, R., Suckling, J., Coleman, M.R., Pickard, J.D., Menon, D., Bullmore, E., 2005. Neurophysiological architecture of functional magnetic resonance images of human brain. *Cereb Cortex* 15(9), 1332-1342.

Schellinger, P.D., Fiebach, J.B., Jansen, O., Ringleb, P.A., Mohr, A., Steiner, T., Heiland, S., Schwab, S., Pohlers, O., Ryssel, H., Orakcioglu, B., Sartor, K., Hacke, W., 2001. Stroke magnetic resonance imaging within 6 hours after onset of hyperacute cerebral ischemia. *Ann Neurol* 49(4), 460-469.

Schellinger, P.D., Latour, L.L., Wu, C.S., Chalela, J.A., Warach, S., 2006. The association between neurological deficit in acute ischemic stroke and mean transit time: comparison of four different perfusion MRI algorithms. *Neuroradiology* 48(2), 69-77.

Schlaug, G., Benfield, A., Baird, A.E., Siewert, B., Lövblad, K.O., Parker, R.A., Edelman, R.R., Warach, S., 1999. The ischemic penumbra: operationally defined by diffusion and perfusion MRI. *Neurology*, 53(7), 1528-1537.

Seeley, W.W., Crawford, R.K., Zhou, J., Miller, B.L., Greicius, M.D., 2009. Neurodegenerative diseases target large-scale human brain networks. *Neuron* 62(1), 42-52.

Shehzad, Z., Kelly, A.M., Reiss, P.T., Gee, D.G., Gotimer, K., Uddin, L.Q., Lee, S.H., Margulies, D.S., Roy, A.K., Biswal, B.B., Petkova, E., Castellanos, F.X., Milham, M.P., 2009. The resting brain: unconstrained yet reliable. *Cereb Cortex* 19(10), 2209-2229.

Smith, S.M., Bandettini, P.A., Miller, K.L., Behrens, T.E., Friston, K.J., David, O., Liu, T., Woolrich, M.W., Nichols, T.E., 2012a. The danger of systematic bias in group-level fMRI-lag-based causality estimation. *Neuroimage* 59(2), 1228-1229.

Smith, S.M., Miller, K.L., Moeller, S., Xu, J., Auerbach, E.J., Woolrich, M.W., Beckmann, C.F., Jenkinson, M., Andersson, J., Glasser, M.F., Van Essen, D.C., Feinberg, D.A., Yacoub, E.S., Ugurbil, K., 2012b. Temporally-independent functional modes of spontaneous brain activity. *Proc Natl Acad Sci U S A* 109(8), 3131-3136.

Sorensen, A.G., Buonanno, F.S., Gonzalez, R.G., Schwamm, L.H., Lev, M.H., Huang-Hellinger, F.R., Reese, T.G., Weisskoff, R.M., Davis, T.L., Suwanwela, N., Can, U., Moreira, J.A., Copen, W.A., Look, R.B., Finklestein, S.P., Rosen, B.R., Koroshetz, W.J., 1996. Hyperacute stroke: evaluation with combined multisection diffusion-weighted and hemodynamically weighted echo-planar MR imaging. *Radiology* 199(2), 391-401.

Sorg, C., Riedl, V., Mühlau, M., Calhoun, V.D., Eichele, T., Läer, L., Drzezga, A., Förstl, F., Kurz, A., Zimmer, C., Wohlschläger, A.M., 2007. Selective changes of resting-state networks in individuals at risk for Alzheimer's disease. *Proc Natl Acad Sci U S A* 104(47), 18760-18765.

Sridharan, D., Levitin, D.J., Menon, V., 2008. A critical role for the right fronto-insular cortex in switching between central-executive and default-mode networks. *Proc Natl Acad Sci U S A* 105(34), 12569-12574.

Starck, T., Remes, J., Nikkinen, J., Tervonen, O., Kiviniemi, V., 2010. Correction of low-frequency physiological noise from the resting state BOLD fMRI-Effect on ICA default mode analysis at 1.5T. *J Neurosci Methods* 186(2), 179-185

Stein, T., Moritz, C., Quigley, M., Cordes, D., Haughton, V., Meyerand, E., 2000. Functional connectivity in the thalamus and hippocampus studied with functional MR imaging. *AJNR Am J Neuroradiol* 21(8), 1397-1401

Stejskal, E.O., Tanner, J.E., 1965. Spin diffusion measurements: spin echoes in the presence of a time-dependent field gradient. *J Chem Phys* 42, 288-292.

Thomas, C.G., Harshman, R.A., Menon, R.S., 2002. Noise reduction in bold-based fMRI using component analysis. *NeuroImage* 17(3), 1521-1537.

Tohka, J., Foerde, K., Aron, A.R., Tom, S.M., Toga, A.W., Poldrack, R.A., 2008. Automatic independent component labeling for artifact removal in fMRI. *NeuroImage* 39(3), 1227-1245.

Tong, Y., Frederick, B.D., 2010. Time lag dependent multimodal processing of concurrent fMRI and near-infrared spectroscopy (NIRS) data suggests a global circulatory origin for low-frequency oscillation signals in human brain. *Neuroimage*

53(2), 553-564.

Thirion, B., Dodel, S., Poline, J.B., 2006. Detection of signal synchronizations in resting-state fMRI datasets. *Neuroimage* 29(1), 321-327.

Uddin, L.Q., Kelly, A.M., Biswal, B.B., Xavier Castellanos, F., Milham, M.P., 2009. Functional connectivity of default mode network components: correlation, anticorrelation, and causality. *Hum Brain Mapp* 30(2), 625-637.

Van De Ven, V.G., Formisano, E., Prvulovic, D., Roeder, C.H., Linden, D.E., 2004. Functional connectivity as revealed by spatial independent component analysis of fMRI measurements during rest. *Hum Brain Mapp* 22, 165-178.

Van den Heuvel, M., Mandl, R., Hulshoff Pol, H., 2008. Normalized cut group clustering of resting-state FMRI data. *PLoS One* 3(4), e2001.

Van Dijk, K.R., Hedden, T., Venkataraman, A., Evans, K.C., Lazar, S.W., Buckner, R.L., 2010. Intrinsic functional connectivity as a tool for human connectomics: theory, properties, and optimization. *J Neurophysiol* 103(1), 297-321.

Villringer, A., Rosen, B.R., Belliveau, J.W., Ackerman, J.L., Lauffer, R.B., Buxton, R.B., Chao, Y.S., Wedeen, V.J., Brady, T.J., 1988. Dynamic imaging with lanthanide chelates in normal brain: contrast due to magnetic susceptibility effects. *Magn Reson Med* 6(2), 164-174.

Warach, S., Chien, D., Li, W., Ronthal, M., Edelman, R.R., 1992. Fast magnetic resonance diffusionweighted imaging of acute human stroke. *Neurology* 42, 1717-1723.

Wardlaw, J.M., 2010. Neuroimaging in acute ischaemic stroke: insights into unanswered questions of pathophysiology. *J Intern Med* 267(2), 172-190.

WHO Task Force 1989. Recommendations on stroke prevention, diagnosis, and therapy. Report of the WHO Task Force on Stroke and other Cerebrovascular Disorders. *Stroke* 20(10), 1407-1431

Wolf, R.C., Sambataro, F., Vasic, N., Schönfeldt-Lecuona, C., Ecker, D., Landwehrmeyer, B., 2008. Aberrant connectivity of lateral prefrontal networks in presymptomatic Huntington's disease. *Exp Neurol* 213 (1), 137-144

Wu, T., Long, X., Zang, Y., Wang, L., Hallett, M., Li, K., Chan, P., 2009. Regional homogeneity changes in patients with Parkinson's disease. *Hum Brain Mapp* 30(5), 1502-1510.

Xiong, J., Parsons, L.M., Gao, J.H., Fox, P.T., 1999. Interregional connectivity to primary motor cortex revealed using MRI resting state images. *Hum Brain Mapp* 8(2-3), 151-156.

Yang, H., Long, X.Y., Yang, Y., Yan, H., Zhu, C.Z., Zhou, X.P., Zang, Y.F., Gong, Q.Y., 2007. Amplitude of low frequency fluctuation within visual areas revealed by resting-state functional MRI. *Neuroimage* 36(1), 144-152.

Yuan, Y., Zhang, Z., Bai, F., Yu, H., Shi, Y., Qian, Y., Liu, W., You, J., Zhang, X., Liu, Z., 2008. Abnormal neural activity in the patients with remitted geriatric depression: a resting-state functional magnetic resonance imaging study. *J Affect Disord* 111(2-3), 145-152.

Zang, Y., Jiang, T., Lu, Y., He, Y., Tian, L., 2004. Regional homogeneity approach to fMRI data analysis. *Neuroimage* 22(1), 394-400.

Zang, Y.F., He, Y., Zhu, C.Z., Cao, Q.J., Sui, M.Q., Liang, M., Tian, L.X., Jiang, T.Z., Wang, Y.F., 2007. Altered baseline brain activity in children with ADHD revealed by restingstate functional MRI. *Brain Dev* 29, 83-91.

Zhang, Z., Lu, G., Zhong, Y., Tan, Q., Yang, Z., Liao, W., Chen, Z., Shi, J., Liu, Y., 2009. Impaired attention network in temporal lobe epilepsy: a resting fMRI study. *Neurosci Lett* 458(3), 97-101.

Zou, Q.H., Zhu, C.Z., Yang, Y., Zuo, X.N., Long, X.Y., Cao, Q.J., Wang, Y.F., Zang, Y.F., 2008. An improved approach to detection of amplitude of low-frequency fluctuation (ALFF) for resting-state fMRI: fractional ALFF. *J Neurosci Methods* 172, 137-141.

Zuo, X.N., Di Martino, A., Kelly, C., Shehzad, Z.E., Gee, D.G., Klein, D.F., Castellanos, F.X., Biswal, B.B., Milham, M.P., 2010a. The oscillating brain: Complex and reliable. *Neuroimage* 49(2), 1432-1445.

Zuo, X.N., Kelly, C., Adelstein, J.S., Klein, D.F., Castellanos, F.X., Milham, M.P., 2010b. Reliable Intrinsic Connectivity Networks: Test-Retest Evaluation Using ICA and Dual Regression Approach. *NeuroImage* 49(3), 2163-2177.

Zuo, X.N., Xu, T., Jiang, L., Yang, Z., Cao, X.Y., He, Y., Zang, Y.F., Castellanos, F.X., Milham, M.P., 2013. Toward reliable characterization of functional homogeneity in the human brain: preprocessing, scan duration, imaging resolution and computational space. *Neuroimage* 65, 374-386.

Acknowledgements

I want to thank Prof. Dr. Arno Villringer, Dr. Daniel S. Margulies and people in resting-state group (Xiangyu Long, Judy Kipping, Alexander Schäfer, Smadar Ovadia) for helping me with my doctoral project. I want to thank Dr. R. Cameron Craddock for helping me develop the time-shift analysis (TSA) method. I want to thank Prof. Dr. Matthias Endres, Dr. Jochen Fiebach, Dr. Kersten Villringer, Dr Benjamin Winter, Daniel Gierhake in the Division of Academic Neuroradiology at Charité Hospital for collecting and delineating the data for my doctoral project. I also want to thank Birgit Mittag, Cornelia Ketscher and Anahit Babayan for helping me during my doctoral study. Thank you.

Yating Lv, Leipzig

Erklärung über die eigenständige Abfassung der Arbeit

Hiermit erkläre ich, dass ich die vorliegende Arbeit selbständig und ohne unzulässige Hilfe oder Benutzung anderer als der angegebenen Hilfsmittel angefertigt habe. Ich versichere, dass Dritte von mir weder unmittelbar noch mittelbar geldwerte Leistungen für Arbeiten erhalten haben, die im Zusammenhang mit dem Inhalt der vorgelegten Dissertation stehen, und dass die vorgelegte Arbeit weder im Inland noch im Ausland in gleicher oder ähnlicher Form einer anderen Prüfungsbehörde zum Zweck einer Promotion oder eines anderen Prüfungsverfahrens vorgelegt wurde. Alles aus anderen Quellen und von anderen Personen übernommene Material, das in der Arbeit verwendet wurde oder auf das direkt Bezug genommen wird, wurde als solches kenntlich gemacht. Insbesondere wurden alle Personen genannt, die direkt an der Entstehung der vorliegenden Arbeit beteiligt waren.

.....
Datum

.....
Unterschrift

CURRICULUM VITAE

PERSONAL INFORMATION:

Name: Yating Lv
Date of Birth: April 7, 1982
Nationality: P.R. China
Place of Birth: Shanxi Province, P.R. China
Language: Chinese, English
Address: Max-Planck-Institut für Kognitions- und Neurowissenschaften
Abteilung Neurologie
Stephanstraße 1A, 04103 Leipzig, Deutschland
Tel: 017668546473
Email: lvating198247@gmail.com, yating@cbs.mpg.de
Homepage: <http://www.cbs.mpg.de/staff/yating-11154>

EDUCATION:

2009 – Now: Doctoral student at Department of Neurology, Max Planck Institute for Human Cognitive and Brain Sciences
Thesis topic: Application of resting-state fMRI methods to acute ischemic stroke.

Supervised by Prof. Dr. Arno Villringer and Dr. Daniel S. Margulies.

Participated project: Stroke project, supported by BMBF (IFB grant to Center for Stroke Research), Einstein Foundation (Mind & Brain Institute), and DFG (Berlin School of Mind and Brain): data processing, results analysis and article writing

2008 – 2009: Research Assistant in Institute of Automation, Chinese Academy of

Science (CASIA).

Participated project: Additional certification of ReHo and ALFF (applying project of National Natural Science Fund): experiment designing and data collecting data processing, results analysis and article writing

2005 - 2008: Master Degree in Engineering, Medical Image Processing, National Laboratory of Pattern Recognition (NLPR), CASIA.

Thesis topic: The study of pianists' brain functions and structures using multi-model neuroimaging.

Supervised by Yu-Feng Zang, M.D.

Participated project: The functional connectivity network of motor cortex in pianist's brain: A fMRI study (applying project of National Natural Science Fund): data processing, results analysis and article writing.

2000 - 2005: Bachelor Degree (Biomedical Engineering)

The College of Biomedical Engineering, Tianjin Medical University (TJMU)

◆ PUBLICATIONS

1. **Lv Y**, Margulies DS, Villringer A, Zang YF. Effects of finger tapping frequency on regional homogeneity of sensorimotor cortex. *PLoS One*, 2013, 8(5): e64115.
2. **Lv Y**, Margulies DS, Cameron Craddock R, Long X, Winter B, Gierhake D, Endres M, Villringer K, Fiebach J, Villringer A. Identifying the perfusion deficit in acute stroke with resting-state functional magnetic resonance imaging. *Ann Neurol*, 2013, 73(1): 136-140.
3. **Lv YT**, Yang H, Wang DY, Li SY, Han Y, Zhu CZ, He Y, Tang HH, Gong QY, Zang YF. Correlations in spontaneous activity and gray matter density between left and right sensorimotor areas of pianists. *NeuroReport*, 2008, 19(6): 631-634
4. Han Y, Yang H, **Lv YT**, Zhu CZ, He Y, Tang HH, Gong QY, Luo YJ, Zang YF, Dong Q. Gray matter density and white matter integrity in pianists' brain: A combined structural and diffusion tensor MRI study. *Neurosci Lett*. 2009 Jul 31; 459(1): 3-6.
5. Cao Q, Sun L, Gong G, **Lv Y**, Cao X, Shuai L, Zhu C, Zang Y, Wang Y. The macrostructural and microstructural abnormalities of corpus callosum in children with attention deficit/hyperactivity disorder: a combined morphometric and diffusion tensor MRI study. *Brain Res*. 2010 Jan 15; 1310: 172-80.
6. Margulies DS, Böttger J, Long X, **Lv Y**, Kelly C, Schäfer A, Goldhahn D, Abbushi A, Milham MP, Lohmann G, Villringer A. Resting developments: a review of fMRI post-processing methodologies for spontaneous brain activity. *MAGMA*. 2010 Dec; 23(5-6): 289-307.
7. Li Y, Ding G, Booth JR, Huang R, **Lv Y**, Zang Y, He Y, Peng D. Sensitive period for white-matter connectivity of superior temporal cortex in deaf people. *Hum Brain Mapp*. 2012 Feb; 33(2): 349-59.
8. Li S, Han Y, Wang D, Yang H, Fan Y, **Lv Y**, Tang H, Gong Q, Zang Y, He Y. Mapping Surface Variability of the Central Sulcus in Musicians. *Cereb Cortex*. 2010 Jan; 20(1): 25-33
9. Liu Z, Xu C, Xu Y, Wang Y, Zhao B, **Lv Y**, Cao X, Zhang K, Du C. Decreased regional homogeneity in insula and cerebellum: a resting-state fMRI study in patients with major depression and subjects at high risk for major depression. *Psychiatry Res*. 2010 Jun 30; 182(3): 211-5.

◆ PRESENTATIONS

1. **Lv Y**, Margulies DS, Zuo X, Villringer A. (2012). Exploring brain structure and function: The relationship between cortical thickness and fMRI BOLD activity. Poster presented at 18th Annual Meeting of the Organization for Human Brain Mapping, Beijing, China.
2. **Lv Y**, Margulies DS, Craddock C, Long X, Winter B, Endres M, Gierhake D, Villringer K, Fiebach J, Villringer A. (2011). Identifying the perfusion deficit in acute stroke with resting-state fMRI. Poster presented at 41th Annual Meeting of the Society for Neuroscience, Washington, USA.

3. **Lv Y**, Margulies DS, Long X, Rohr C, Winter B, Endres M, Villringer K, Fiebach J, Villringer A. (2011). Tissue-Differentiation in Stroke using resting-state fMRI. Poster presented at 17th Annual Meeting of the Organization for Human Brain Mapping, Quebec, Canada.

4. **Lv Y**, Long X, Margulies DS, Villringer A, Zang Y. (2010). Finger tapping effect on regional homogeneity of sensorimotor cortex. Poster presented at 16th Annual Meeting of the Organization for Human Brain Mapping, Barcelona, Spain.

5. **Lv Y**, Margulies DS, Winter B, Rohr C, Lachmann C, Lohmann G, Kunze C, Brunecker P, Villringer K, Endres M, Fiebach J, Villringer A. (2010). A novel method for detecting post-stroke functional tissue damage using resting-state fMRI. Poster presented at 16th Annual Meeting of the Organization for Human Brain Mapping, Barcelona, Spain.

◆ **PATENT**

Arno Vilringer, Daniel S. Margulies, **Yating Lv**, Richard Cameron Craddock. Inventor of “Method and apparatus for visualization of tissue perfusion by means of assessing BOLD signal fluctuations”. European Patent Office.